EUROPEAN ORGANISATION FOR NUCLEAR RESEARCH

CERN-PPE/96-096
15 July 1996

Searches for Supersymmetric Particles and Anomalous Four-Jet Production at $\sqrt{s} = 130$ and 136 GeV at LEP

The OPAL Collaboration

Abstract

A search for supersymmetric particles (charged scalar leptons, charginos decaying semileptonically, scalar top quarks) and for the associated production of two massive particles decaying into quarks has been performed using a data sample of more than 5 pb^{-1} at centre-of-mass energies of $\sqrt{s}$ =130 and 136 GeV collected with the OPAL detector at LEP during November 1995. No evidence for production of any of these particles has been observed in the data. Limits are presented on the production of charged scalar leptons, semileptonically decaying charginos, scalar top quarks and on the associated production of two massive particles leading to four-jet final states.

(Submitted to Zeitschrift f. Physik)

The OPAL Collaboration

G. Alexander[23], J. Allison[16], N. Altekamp[5], K. Ametewee[25], K.J. Anderson[9], S. Anderson[12], S. Arcelli[2], S. Asai[24], D. Axen[29], G. Azuelos[18,a], A.H. Ball[17], E. Barberio[8], R.J. Barlow[16], R. Bartoldus[3], J.R. Batley[5], J. Bechtluft[14], C. Beeston[16], T. Behnke[8], A.N. Bell[1], K.W. Bell[20], G. Bella[23], S. Bentvelsen[8], P. Berlich[10], S. Bethke[14], O. Biebel[14], V. Blobel[8], I.J. Bloodworth[1], J.E. Bloomer[1], M. Bobinski[10], P. Bock[11], H.M. Bosch[11], M. Boutemeur[34], B.T. Bouwens[12], S. Braibant[12], R.M. Brown[20], H.J. Burckhart[8], C. Burgard[8], R. Bürgin[10], P. Capiluppi[2], R.K. Carnegie[6], A.A. Carter[13], J.R. Carter[5], C.Y. Chang[17], C. Charlesworth[6], D.G. Charlton[1,b], D. Chrisman[4], S.L. Chu[4], P.E.L. Clarke[15], I. Cohen[23], J.E. Conboy[15], O.C. Cooke[16], M. Cuffiani[2], S. Dado[22], C. Dallapiccola[17], G.M. Dallavalle[2], S. De Jong[12], L.A. del Pozo[8], K. Desch[3], M.S. Dixit[7], E. do Couto e Silva[12], M. Doucet[18], E. Duchovni[26], G. Duckeck[34], I.P. Duerdoth[16], J.E.G. Edwards[16], P.G. Estabrooks[6], H.G. Evans[9], M. Evans[13], F. Fabbri[2], P. Fath[11], F. Fiedler[12], M. Fierro[2], H.M. Fischer[3], R. Folman[26], D.G. Fong[17], M. Foucher[17], A. Fürtjes[8], P. Gagnon[7], A. Gaidot[21], J.W. Gary[4], J. Gascon[18], S.M. Gascon-Shotkin[17], N.I. Geddes[20], C. Geich-Gimbel[3], F.X. Gentit[21], T. Geralis[20], G. Giacomelli[2], P. Giacomelli[4], R. Giacomelli[2], V. Gibson[5], W.R. Gibson[13], D.M. Gingrich[30,a], D. Glenzinski[9], J. Goldberg[22], M.J. Goodrick[5], W. Gorn[4], C. Grandi[2], E. Gross[26], M. Gruwé[8], C. Hajdu[32], G.G. Hanson[12], M. Hansroul[8], M. Hapke[13], C.K. Hargrove[7], P.A. Hart[9], C. Hartmann[3], M. Hauschild[8], C.M. Hawkes[5], R. Hawkings[8], R.J. Hemingway[6], G. Herten[10], R.D. Heuer[8], M.D. Hildreth[8], J.C. Hill[5], S.J. Hillier[1], T. Hilse[10], P.R. Hobson[25], R.J. Homer[1], A.K. Honma[28,a], D. Horváth[32,c], R. Howard[29], R.E. Hughes-Jones[16], D.E. Hutchcroft[5], P. Igo-Kemenes[11], D.C. Imrie[25], M.R. Ingram[16], K. Ishii[24], A. Jawahery[17], P.W. Jeffreys[20], H. Jeremie[18], M. Jimack[1], A. Joly[18], C.R. Jones[5], G. Jones[16], M. Jones[6], R.W.L. Jones[8], U. Jost[11], P. Jovanovic[1], T.R. Junk[8], D. Karlen[6], K. Kawagoe[24], T. Kawamoto[24], R.K. Keeler[28], R.G. Kellogg[17], B.W. Kennedy[20], B.J. King[8], J. Kirk[29], S. Kluth[8], T. Kobayashi[24], M. Kobel[10], D.S. Koetke[6], T.P. Kokott[3], S. Komamiya[24], R. Kowalewski[8], T. Kress[11], P. Krieger[6], J. von Krogh[11], P. Kyberd[13], G.D. Lafferty[16], H. Lafoux[21], R. Lahmann[17], W.P. Lai[19], D. Lanske[14], J. Lauber[15], S.R. Lautenschlager[31], J.G. Layter[4], D. Lazic[22], A.M. Lee[31], E. Lefebvre[18], D. Lellouch[26], J. Letts[2], L. Levinson[26], C. Lewis[15], S.L. Lloyd[13], F.K. Loebinger[16], G.D. Long[17], M.J. Losty[7], J. Ludwig[10], A. Luig[10], A. Malik[21], M. Mannelli[8], S. Marcellini[2], C. Markus[3], A.J. Martin[13], J.P. Martin[18], G. Martinez[17], T. Mashimo[24], W. Matthews[25], P. Mättig[3], W.J. McDonald[30], J. McKenna[29], E.A. Mckigney[15], T.J. McMahon[1], A.I. McNab[13], R.A. McPherson[8], F. Meijers[8], S. Menke[3], F.S. Merritt[9], H. Mes[7], J. Meyer[27], A. Michelini[2], G. Mikenberg[26], D.J. Miller[15], R. Mir[26], W. Mohr[10], A. Montanari[2], T. Mori[24], M. Morii[24], U. Müller[3], K. Nagai[26], I. Nakamura[24], H.A. Neal[8], B. Nellen[3], B. Nijjhar[16], R. Nisius[8], S.W. O'Neale[1], F.G. Oakham[7], F. Odorici[2], H.O. Ogren[12], T. Omori[24], M.J. Oreglia[9], S. Orito[24], J. Pálinkás[33,d], G. Pásztor[32], J.R. Pater[16], G.N. Patrick[20], J. Patt[10], M.J. Pearce[1], S. Petzold[27], P. Pfeifenschneider[14], J.E. Pilcher[9], J. Pinfold[30], D.E. Plane[8], P. Poffenberger[28], B. Poli[2], A. Posthaus[3], H. Przysiezniak[30], D.L. Rees[1], D. Rigby[1], S.A. Robins[13], N. Rodning[30], J.M. Roney[28], A. Rooke[15], E. Ros[8], A.M. Rossi[2], M. Rosvick[28], P. Routenburg[30], Y. Rozen[22], K. Runge[10], O. Runolfsson[8], U. Ruppel[14], D.R. Rust[12], R. Rylko[25], K. Sachs[10], E.K.G. Sarkisyan[23], M. Sasaki[24], C. Sbarra[2], A.D. Schaile[34], O. Schaile[34], F. Scharf[3], P. Scharff-Hansen[8], P. Schenk[4], B. Schmitt[8], S. Schmitt[11], M. Schröder[8], H.C. Schultz-Coulon[10], M. Schulz[8], M. Schumacher[3], P. Schütz[3], W.G. Scott[20], T.G. Shears[16], B.C. Shen[4], C.H. Shepherd-Themistocleous[27], P. Sherwood[15], G.P. Siroli[2], A. Sittler[27], A. Skillman[15], A. Skuja[17], A.M. Smith[8], T.J. Smith[28], G.A. Snow[17], R. Sobie[28], S. Söldner-Rembold[10], R.W. Springer[30], M. Sproston[20], A. Stahl[3],

M. Starks[12], M. Steiert[11], K. Stephens[16], J. Steuerer[27], B. Stockhausen[3], D. Strom[19], F. Strumia[8], P. Szymanski[20], R. Tafirout[18], S.D. Talbot[1], S. Tanaka[24], P. Taras[18], S. Tarem[22], M. Tecchio[8], M. Thiergen[10], M.A. Thomson[8], E. von Törne[3], S. Towers[6], T. Tsukamoto[24], E. Tsur[23], A.S. Turcot[9], M.F. Turner-Watson[8], P. Utzat[11], R. Van Kooten[12], G. Vasseur[21], M. Verzocchi[10], P. Vikas[18], M. Vincter[28], E.H. Vokurka[16], F. Wäckerle[10], A. Wagner[27], C.P. Ward[5], D.R. Ward[5], J.J. Ward[15], P.M. Watkins[1], A.T. Watson[1], N.K. Watson[7], P. Weber[6], P.S. Wells[8], N. Wermes[3], J.S. White[28], B. Wilkens[10], G.W. Wilson[27], J.A. Wilson[1], G. Wolf[26], S. Wotton[5], T.R. Wyatt[16], S. Yamashita[24], G. Yekutieli[26], V. Zacek[18],

[1]School of Physics and Space Research, University of Birmingham, Birmingham B15 2TT, UK
[2]Dipartimento di Fisica dell' Università di Bologna and INFN, I-40126 Bologna, Italy
[3]Physikalisches Institut, Universität Bonn, D-53115 Bonn, Germany
[4]Department of Physics, University of California, Riverside CA 92521, USA
[5]Cavendish Laboratory, Cambridge CB3 0HE, UK
[6] Ottawa-Carleton Institute for Physics, Department of Physics, Carleton University, Ottawa, Ontario K1S 5B6, Canada
[7]Centre for Research in Particle Physics, Carleton University, Ottawa, Ontario K1S 5B6, Canada
[8]CERN, European Organisation for Particle Physics, CH-1211 Geneva 23, Switzerland
[9]Enrico Fermi Institute and Department of Physics, University of Chicago, Chicago IL 60637, USA
[10]Fakultät für Physik, Albert Ludwigs Universität, D-79104 Freiburg, Germany
[11]Physikalisches Institut, Universität Heidelberg, D-69120 Heidelberg, Germany
[12]Indiana University, Department of Physics, Swain Hall West 117, Bloomington IN 47405, USA
[13]Queen Mary and Westfield College, University of London, London E1 4NS, UK
[14]Technische Hochschule Aachen, III Physikalisches Institut, Sommerfeldstrasse 26-28, D-52056 Aachen, Germany
[15]University College London, London WC1E 6BT, UK
[16]Department of Physics, Schuster Laboratory, The University, Manchester M13 9PL, UK
[17]Department of Physics, University of Maryland, College Park, MD 20742, USA
[18]Laboratoire de Physique Nucléaire, Université de Montréal, Montréal, Quebec H3C 3J7, Canada
[19]University of Oregon, Department of Physics, Eugene OR 97403, USA
[20]Rutherford Appleton Laboratory, Chilton, Didcot, Oxfordshire OX11 0QX, UK
[21]CEA, DAPNIA/SPP, CE-Saclay, F-91191 Gif-sur-Yvette, France
[22]Department of Physics, Technion-Israel Institute of Technology, Haifa 32000, Israel
[23]Department of Physics and Astronomy, Tel Aviv University, Tel Aviv 69978, Israel
[24]International Centre for Elementary Particle Physics and Department of Physics, University of Tokyo, Tokyo 113, and Kobe University, Kobe 657, Japan
[25]Brunel University, Uxbridge, Middlesex UB8 3PH, UK
[26]Particle Physics Department, Weizmann Institute of Science, Rehovot 76100, Israel
[27]Universität Hamburg/DESY, II Institut für Experimental Physik, Notkestrasse 85, D-22607 Hamburg, Germany
[28]University of Victoria, Department of Physics, P O Box 3055, Victoria BC V8W 3P6, Canada
[29]University of British Columbia, Department of Physics, Vancouver BC V6T 1Z1, Canada

[30]University of Alberta, Department of Physics, Edmonton AB T6G 2J1, Canada
[31]Duke University, Dept of Physics, Durham, NC 27708-0305, USA
[32]Research Institute for Particle and Nuclear Physics, H-1525 Budapest, P O Box 49, Hungary
[33]Institute of Nuclear Research, H-4001 Debrecen, P O Box 51, Hungary
[34]Ludwigs-Maximilians-Universität München, Sektion Physik, Am Coulombwall 1, D-85748 Garching, Germany

[a] and at TRIUMF, Vancouver, Canada V6T 2A3
[b] and Royal Society University Research Fellow
[c] and Institute of Nuclear Research, Debrecen, Hungary
[d] and Department of Experimental Physics, Lajos Kossuth University, Debrecen, Hungary

1 Introduction

We have searched for leptonic and hadronic events with missing energy and for new particles in four-jet final states, in e^+e^- collisions at centre-of-mass energies of $\sqrt{s}$ = 130–136 GeV (LEP 1.5). The searches with missing energy topologies are designed to select new particles predicted by supersymmetric theories: charged scalar leptons, charginos that decay semileptonically, and scalar top quarks. The four-jet search is sensitive to the production of two massive particles, X and Y, both decaying to two jets. This topology may be produced by processes such as $e^+e^- \to A^0h^0$ or $e^+e^- \to H^+H^-$, where A^0, h^0, and $H^\pm$ are Higgs bosons required by any model with at least two Higgs doublets such as Supersymmetry. It is also particularly of interest as the ALEPH collaboration has recently reported [1] an excess of events with the sum of dijet masses consistent with $(m_X + m_Y) \simeq 105$ GeV for $m_X \approx m_Y$. The data sample considered was collected in autumn 1995 with the OPAL detector, at energies well above the Z peak and provided an opportunity to search for new particles at the highest energies available at e^+e^- colliders, but below the $e^+e^- \to W^+W^-$ threshold.

In models invoking Supersymmetry (SUSY) [2] each elementary particle is accompanied by a supersymmetric partner whose spin differs by half a unit. SUSY models require a minimum of two Higgs doublets to generate the masses of bosons and fermions. In SUSY models with two Higgs doublets, the fields of the fermionic partners of the $W^\pm$ and of the charged Higgs bosons, $H^\pm$, mix to form two mass eigenstates, the charginos $\tilde{\chi}^\pm_{1,2}$. The fields of the partners of the γ, of the Z^0 and of the neutral Higgs bosons mix to form four mass eigenstates, the neutralinos $\tilde{\chi}^0_i$ ($i = 1,...,4$, in increasing mass order). In the following we will make the assumption that a new multiplicative quantum number, R-parity [3], which discriminates between ordinary and supersymmetric particles, is conserved and that the lightest neutralino, $\tilde{\chi}^0_1$, is the lightest supersymmetric particle (LSP). R-parity conservation implies that supersymmetric particles are always pair-produced and always decay, through cascade decays, to ordinary particles and $\tilde{\chi}^0_1$. The $\tilde{\chi}^0_1$ is stable and escapes detection due to its weakly interacting nature. Therefore a characteristic signature of all events containing supersymmetric particles when R-parity is conserved is missing energy and unbalanced momentum.

In SUSY theories, each lepton has two scalar partners, the right- and left-handed scalar leptons (sleptons) denoted $\tilde{\ell}_R$ and $\tilde{\ell}_L$, according to the helicity states of their non-SUSY partners. Sleptons could be pair-produced through s-channel Z^0 or γ exchange. Scalar electrons (selectrons, $\tilde{e}$) could also be produced through t-channel neutralino exchange enhancing the selectron production cross-section compared to the scalar muon (smuon, $\tilde{\mu}$) and scalar tau (stau, $\tilde{\tau}$) production cross-sections. The next-to-lightest neutralino $\tilde{\chi}^0_2$ and the lightest charginos $\tilde{\chi}^\pm_1$ were, for the purpose of our slepton searches, assumed to be heavier than the sleptons. The dominant slepton decay mode would therefore be expected to be $\tilde{\ell}^\pm \to \ell^\pm + \tilde{\chi}^0_1$.

Charginos could be pair produced in e^+e^- collisions through s-channel Z^0 or γ exchange and t-channel sneutrino ($\tilde{\nu}_e$) exchange. Charginos would decay via exchange of a virtual W, squarks, sleptons or charged Higgs bosons into $\tilde{\chi}^0_1 f\overline{f}'$ where f is a quark or lepton. We have already reported on a general search for charginos [4], and we present here an update on the search for the semileptonic decay of the chargino with decay products $\tilde{\chi}^\pm_1 \to \tilde{\chi}^0_1 \ell^\pm \nu$ proceeding via a virtual W, a real or virtual slepton $\tilde{\chi}^\pm_1 \to \tilde{\ell}^{(*)}\nu$, or a real or virtual sneutrino $\tilde{\chi}^\pm_1 \to \tilde{\nu}^{(*)}\ell^\pm$.

The scalar top quark (stop, $\tilde{\mathrm{t}}$), the bosonic partner of the top quark, could be the lightest charged supersymmetric (SUSY) particle for two reasons [5, 6]. Firstly, one loop radiative corrections to the $\tilde{\mathrm{t}}$ mass through Higgsino-quark loops and Higgs-squark loops are always negative. The correction is large for a large top quark mass of about 180 GeV [7]. Secondly, the supersymmetric partners of the right-handed and left-handed top quarks ($\tilde{\mathrm{t}}_\mathrm{L}$ and $\tilde{\mathrm{t}}_\mathrm{R}$) mix, and the resultant two mass eigenstates ($\tilde{\mathrm{t}}_1$ and $\tilde{\mathrm{t}}_2$) have a large mass splitting. The lighter mass eigenstate ($\tilde{\mathrm{t}}_1$) could be lighter than any other charged SUSY particle, and lighter than the top quark itself [5, 6]. The stop quark pair-production cross-section depends on the stop mass, $m_{\tilde{\mathrm{t}}_1}$, and the mixing angle θ_{mix}, where $\tilde{\mathrm{t}}_1 = \tilde{\mathrm{t}}_\mathrm{L}\cos\theta_{\mathrm{mix}} + \tilde{\mathrm{t}}_\mathrm{R}\sin\theta_{\mathrm{mix}}$. For the stop search, the stop quark is assumed to be lighter than all other charged SUSY particles, in which case the dominant decay mode would be $\tilde{\mathrm{t}}_1 \to \mathrm{c} + \tilde{\chi}^0_1$.

Other relevant limits on supersymmetric particle production exist from the Tevatron [8, 9], HERA [10], and in $\mathrm{e^+e^-}$ collisions at $\sqrt{s} = 130$–140 GeV from the other LEP collaborations [11].

In the following, the Minimal Supersymmetric extension of the Standard Model (MSSM) [12] is used as a reference model, although the analyses reported here are also valid in a broader context. In the framework of the MSSM, under the assumption of a common scalar mass m_0 at the Grand Unification (GUT) scale, all sparticle masses (but not the Higgs boson masses) and couplings are completely determined by m_0 and a set of four parameters: M_2, the SU(2) gaugino mass parameter at electroweak scales[1]; μ, the mixing parameter of the two Higgs doublets; $\tan\beta = v_2/v_1$, the ratio of the vacuum expectation values for the two Higgs doublets; and A, the trilinear coupling in the Higgs sector.

This paper is organised as follows: we first briefly describe the OPAL detector and the Monte Carlo samples used by the various analyses. We then report on a search for charged sleptons ($\tilde{\mathrm{e}}$, $\tilde{\mu}$ and $\tilde{\tau}$) using two complementary and independent analyses. The first analysis requires two identified electrons or muons that are not back-to-back, while the second searches for dilepton events with missing energy where one lepton (e, μ or τ) is required to pass strict identification requirements while much looser requirements are placed on the second lepton. The latter analysis achieves a higher sensitivity and is also used to search for charginos that decay semileptonically. We then present a search for stop quarks using an analysis similar to the one described in a previous publication [4]. We also describe the search for the associated production of two massive particles, each decaying into quarks leading to a four-jet final state. For this search we also used two analyses, the first one optimised to search for events of the type $\mathrm{e^+e^-} \to \mathrm{XY}$, while the second one is similar to an analysis presented by the ALEPH collaboration [1].

2 The OPAL detector

A complete description of the OPAL detector can be found in Ref. [13] and only detectors relevant to the current analyses are described here.

The central detector consists of a system of tracking chambers providing charged particle

[1] We assume that M_1, the U(1) gaugino mass at electroweak scales, is related to M_2 by the usual gauge unification condition: $M_1 = \frac{5}{3}\tan^2\theta_W M_2$.

tracking over 96% of the full solid angle[2] inside a 0.435 T uniform magnetic field parallel to the beam axis. It consists of a two-layer silicon microstrip vertex detector, a high precision drift chamber, a large volume jet chamber and a set of z chambers measuring the track coordinates along the beam direction. A lead-glass electromagnetic (EM) calorimeter located outside the magnet coil covers the full azimuthal range with excellent hermeticity in the polar angle range of $|\cos\theta| < 0.82$ for the barrel region and $0.81 < |\cos\theta| < 0.984$ for the endcap region. The magnet return yoke is instrumented for hadron calorimetry (HCAL) and consists of barrel and endcap sections along with pole tip detectors that together cover the region $|\cos\theta| < 0.99$. Four layers of muon chambers cover the outside of the hadron calorimeter. Electromagnetic calorimeters close to the beam axis complete the geometrical acceptance down to 24 mrad. These include the forward detectors (FD) which are lead-scintillator sandwich calorimeters and, at smaller angles, silicon tungsten calorimeters (SW) [14] located on both sides of the interaction point. The gap between the endcap EM calorimeter and the FD is instrumented with an additional lead-scintillator electromagnetic calorimeter, called the gamma-catcher.

3 Monte Carlo simulation

The Monte Carlo program SUSYGEN [15] was used to generate samples of $\tilde{e}^+\tilde{e}^-$ and $\tilde{\mu}^+\tilde{\mu}^-$ simulated events for various slepton and neutralino mass combinations. The SUSYGEN generator includes initial state radiation but not final state radiation. The JETSET 7.4 generator [16] including initial state radiation was used to simulate $\tilde{\tau}^+\tilde{\tau}^-$ events. Samples of 1000 $\tilde{\ell}^+\tilde{\ell}^-$ events were generated for each of 25 combinations of $(m_{\tilde{\ell}}^{\pm}, m_{\tilde{\chi}_1^0})$ at $\sqrt{s} = 133$ GeV.

A Monte Carlo program based on the calculation of the differential cross-section by Bartl et al. [17] was used to generate samples of chargino pair events. The charginos were forced to decay semileptonically to $\tilde{\chi}_1^0\ell\nu$ with interference included between decays via virtual sleptons or sneutrinos. We generated 1000 $\tilde{\chi}_1^+\tilde{\chi}_1^-$ events at each of 30 points in the $m_{\tilde{\chi}_1^+}$, Δm ($\Delta m \equiv m_{\tilde{\chi}_1^+} - m_{\tilde{\chi}_1^0}$) plane at $\sqrt{s}$ =133 GeV.

The stop quark Monte Carlo simulation was performed as follows. $\tilde{t}_1\bar{\tilde{t}}_1$ pairs were generated taking into account initial state radiation [16]. The hadronisation process subsequently producing colourless $\tilde{t}_1$-hadrons and other fragmentation products was performed according to the Lund string fragmentation scheme [16]. The $\tilde{t}_1$-hadron was composed of a $\tilde{t}_1$ and a spectator antiquark or a diquark [18]. The $\tilde{t}_1$ decayed into a charm quark, which then hadronised following the Lund string fragmentation scheme [16], and a $\tilde{\chi}_1^0$. We generated 1000 $\tilde{t}_1\bar{\tilde{t}}_1$ events for each of 42 combinations of $(m_{\tilde{t}_1}, m_{\tilde{\chi}_1^0})$ at $\sqrt{s} = 136$ GeV, and for 20 combinations at $\sqrt{s} =$ 130 GeV.

For the search for the associated production of two massive particles we used as signal samples events of the type $e^+e^- \rightarrow A^0h^0$ generated using the program described in Ref. [19] where both the A^0 and h^0 were forced to decay with a branching ratio of 100% to a $b\bar{b}$ system.

[2]The OPAL coordinate system is defined so that the z axis is in the direction of the electron beam, the x axis is horizontal and points towards the centre of the LEP ring; θ and ϕ are the polar and azimuthal angles, defined relative to the $+z$- and $+x$-axes, respectively. The radial coordinate is denoted as r.

We have considered several Standard Model processes as potential background sources. Two-photon processes producing leptonic final states can be an important background for the dilepton searches, while hadronic final states are important for the search for stop quarks. The Vermaseren [20] generator was used to estimate the background contribution from two-photon processes with $e^+e^-\ell^+\ell^-$ final states. In the generation of these samples, it was required that at least one fermion was produced at $|\cos\theta| < 0.97$ and with a transverse momentum with respect to the beam axis, p_t, greater than 1 GeV. It was also required that the invariant mass of the lowest mass fermion pair be greater than 200 MeV. We used the PYTHIA [16] Monte Carlo generator to generate hadronic events from two-photon processes where the virtual mass Q^2 of both photons is smaller than 1.3 GeV^2 and the invariant mass of the photon-photon system ($m_{\gamma\gamma}$) is greater than 3 GeV. For higher Q^2 events, the TWOGEN [21] generator was used. Event samples for all the possible processes were generated, i.e., final state hadrons from point-like $\gamma\gamma \to q\bar{q}$ processes and from vector meson dominance.

The KORALZ [22] event generator was used for the generation of $\mu^+\mu^-(\gamma)$ and $\tau^+\tau^-(\gamma)$ events and the BABAMC [23] and TEEGG [24] event generators were used for the generation of $e^+e^-(\gamma)$ events. $\tau^+\tau^-(\gamma)$ events are a potential source of background for the topology of two acollinear leptons because neutrinos emitted from τ-decays carry away energy and momentum.

The PYTHIA 5.7 program and JETSET 7.4 parton shower generator [16] were used to simulate multihadronic events.

Finally, four-fermion processes in which at least one fermion is a neutrino constitute a potentially serious background to SUSY events with large missing momentum. Since the interference effects of many diagrams are important below the W^+W^- threshold, we used an event generator based on helicity amplitude calculations, which took into account all the relevant diagrams and interference effects [25]. The package also included initial state photon radiation. It was checked that Monte Carlo samples of four-fermion events produced with the EXCALIBUR [26] generator gave similar background estimates.

All generated events were processed through the full simulation of the OPAL detector [27], and the same event analysis chain was applied to simulated events as to the data.

4 Charged scalar leptons (sleptons)

The slepton decay considered is $\tilde{\ell}^\pm \to \ell^\pm + \tilde{\chi}_1^0$, where $\ell^\pm$ is the corresponding charged lepton. The typical experimental signature for slepton pair production would therefore be a pair of charged leptons of the same flavour that are not back-to-back, accompanied by a large missing momentum carried away by the neutralinos. A number of Standard Model processes can lead to large missing energy due to particles escaping undetected along the beam direction. Therefore, a significant missing momentum in the plane perpendicular to the beam axis ($p_t^{\rm miss}$) is required.

In this section, two independent analyses are presented. Analysis A, which is described in subsection 4.1 is focused on a search for selectrons and smuons requiring two identified electrons or muons in the event. Analysis B described in subsection 4.2, presents a more general approach searching for low-multiplicity events containing isolated electrons, muons or

taus in association with significant missing transverse momentum. It requires at least one track to satisfy requirements on lepton identification, isolation and p_t. To maintain a high efficiency, looser requirements are made on the possible presence of a second lepton in the event. If the mass difference between $\tilde{\ell}^{\pm}$ and $\tilde{\chi}_1^0$ is small (< 2 GeV), the visible energy as well as the transverse momentum becomes small. Both analyses were designed to maintain reasonable efficiency also for these difficult cases of small mass differences. Since Analysis B obtains a higher efficiency and better background rejection than Analysis A, Analysis B is used to set the limits for all slepton species, including staus. Nevertheless, the more straightforward Analysis A provides a complementary technique and valuable cross check in case a signal is found. Analysis B has also been used to search for events containing charginos that decay semileptonically and the results are presented in section 5.

The data sample used for the slepton searches consisted of 2.5 pb^{-1} at $\sqrt{s} = 130$ GeV and 2.6 pb^{-1} at $\sqrt{s} = 136$ GeV. To be considered in the analyses, tracks in the central detector and clusters in the electromagnetic calorimeter were required to satisfy the normal quality criteria employed in the analysis of Standard Model lepton pairs [28] (these tracks are hereafter referred to as good tracks). Cosmic rays were rejected using an algorithm described in Ref. [28].

In both of the following analyses, algorithms were adopted which avoid the double-counting of calorimeter energy deposits associated with charged particles, similar to the procedure followed in Ref. [29]. Electron identification included the consideration of ionisation energy loss $\mathrm{d}E/\mathrm{d}x$ measurements of a track in the jet chamber, the match of track momentum with energy deposits in the EM calorimeter, and other measurements from the calorimeters. Muons were identified by associating track segments in the outer muon detectors or HCAL signals with tracks in the central detector and by matching high momentum tracks to energy deposits consistent with a minimum ionising particle in the EM calorimeter. Lepton identification for each of the two analyses is given in detail below.

4.1 Analysis A: selection criteria

First, cuts were applied to veto multihadronic and Bhabha scattering events. Events were rejected if the sum of the number of good tracks in the central detector and the number of clusters in the electromagnetic calorimeter was greater than 18. Bhabha scattering events were identified and then vetoed as described in Ref. [30].

After applying these vetoes, charged tracks were required to pass the above mentioned track quality criteria with the only difference being that the number of hits in the central detector used for the reconstruction of a track was increased from 20 to 40.

The number of good charged tracks was required to be at least two, and the ratio of the number of good tracks to the total number of tracks was required to be greater than 0.2 to reduce backgrounds from beam-gas and beam-wall events. The visible energy and the total transverse momentum of the event were calculated using the method described in Ref. [29].

To select slepton-pair candidate events, the following criteria were applied:

1. To reduce the background from two-photon processes and multihadronic events, the total

energy deposited had to be less than 5 GeV in each silicon tungsten calorimeter, less than 2 GeV in each forward calorimeter, and less than 5 GeV in each side of the gamma-catcher.

2. The background from two-photon processes and "radiative return" events ($e^+e^- \to Z\gamma$) where the γ escaped along the beam direction was reduced by requiring that the polar angle of the missing momentum direction, $\theta_{\rm miss}$, satisfied $|\cos\theta_{\rm miss}| < 0.9$. Figure 1a shows the $\theta_{\rm miss}$ distribution after cut (1) has been applied.

3. The background from beam-gas and two-photon events was also reduced by requiring that $m_{\rm vis}/\sqrt{s} > 0.01$, where $m_{\rm vis}$ is the visible mass of the event. It was also required that $m_{\rm vis}/\sqrt{s} < 0.80$ to reduce the residual background from Bhabha scattering events and yet still retain slepton-pair events with a large mass difference between the slepton and neutralino. Figure 1b shows the distribution of the event visible mass after cuts (1) to (2) have been applied.

4. Most of the remaining events from two-photon processes were rejected by requiring that the missing transverse momentum of the event, $p_t^{\rm miss}$, be greater than 2 GeV and that the missing transverse momentum, including the hadron calorimeter $p_{t,\rm HCAL}^{\rm miss}$, be greater than 3 GeV. The $p_{t,\rm HCAL}^{\rm miss}$ cut was applied to reject two-photon events with an occasional high transverse momentum neutral hadron. Figure 1c shows the $p_{t,\rm HCAL}^{\rm miss}$ distribution after cuts (1) to (3) have been applied.

5. Events were required to contain exactly two or four charged tracks, including at least two identified and oppositely charged leptons (electrons or muons, not necessarily of the same flavour) with $p_t > 1$ GeV, to select the signal. Each of the two possible extra tracks was also required to have $p_t > 0.7$ GeV.

   Electrons were identified if any of the following criteria were satisfied: a loose cut on the output of a neural net electron identification algorithm as described in Ref. [31]; $0.5 < E/p < 2$, where p is the momentum of the track and E is the energy of the associated electromagnetic cluster; or electron requirements described in Ref. [32] and in Ref. [33].

   Muons were identified using the criteria described in Ref. [32].

6. The acoplanarity angle[3] ($\phi_{\rm acop}$) between the two leptons was required to be greater than 20° to reject lepton pair events, and smaller than 175° to reduce the background due to photon conversions. The acoplanarity angle distribution is shown in Fig. 1d after cuts (1) to (5) have been applied. The acollinearity angle[4] ($\phi_{\rm acol}$) was also required to be greater than 20° and smaller than 175°.

7. To reduce the background due to radiative leptonic events with an acollinear pair of leptons in the final state plus one energetic photon, it was required that there be no unassociated electromagnetic cluster with an energy larger than 5 GeV in the final state.

The efficiency for $\tilde{\ell}^+\tilde{\ell}^-$ events is above 60% for $m_{\tilde{\ell}^\pm} = 55$ GeV and $m_{\tilde{\chi}_1^0} = 45$ GeV. In the difficult regions of a small mass difference $\Delta m = (m_{\tilde{\ell}^\pm} - m_{\tilde{\chi}_1^0}) = 2$ GeV, the efficiency is

[3]The acoplanarity angle, $\phi_{\rm acop}$ is defined as the complement of the angle between the directions of the momenta of the two lepton candidates in the $x-y$ plane.

[4]The acollinearity angle, $\phi_{\rm acol}$ is defined as the complement of the three-dimensional angle between the directions of the momenta of the two lepton candidates.

	Data	Total Backg.	$f\bar{f}(\gamma)$	$e^+e^-f\bar{f}$	4-f	$\tilde{\mu}^+\tilde{\mu}^-$ (%)	
$m_{\tilde{\mu}}$ (GeV)						60	60
Δm (GeV)						5	$m_{\tilde{\mu}}/2$
Vetoes	36365	31431.8	525.6	30902.4	3.9	93.4	93.2
cut (1)	25322	22951.1	416.6	22531.1	3.5	92.0	91.9
cut (2)	9830	7778.7	172.4	7603.5	2.8	83.7	85.7
cut (3)	8715	7144.0	113.5	7028.4	2.0	82.4	85.4
cut (4)	243	248.3	95.5	150.9	2.0	72.9	85.2
cut (5)	51	72.5	46.7	25.1	0.8	62.9	75.9
cut (6)	1	4.6	3.5	0.6	0.6	58.7	66.3
cut (7)	0	1.2	0.1	0.6	0.5	58.6	66.0

Table 1: *Analysis A: The remaining numbers of events normalised to the integrated luminosity of the data for various Monte Carlo background processes are compared with data (first column) after each cut. Efficiencies for two simulated event samples of $\tilde{\mu}^+\tilde{\mu}^-$ are also given (last two columns) for two possible values of Δm.*

still about 20%. The numbers of events remaining after each cut are listed in Table 1. For comparison, the table also shows the corresponding numbers of simulated events for background processes and for two samples of simulated $\tilde{\ell}^+\tilde{\ell}^-$ events. There is reasonable agreement between the numbers of events in the data sample and the corresponding numbers of events expected from background processes once the two-photon processes leading to hadronic final states have been effectively removed (after cut (4)). Before this stage the differences between the numbers of events in the data and in the background processes can be explained by the fact that two-photon processes with hadronic final states have not been simulated for an invariant mass of the photon-photon system smaller than 3 GeV.

No events were observed in the data after the above cuts, which is compatible with the expected 1.2 ± 0.4 background events estimated from the Monte Carlo simulations.

4.2 Analysis B: selection criteria

This analysis used tracks reconstructed in the central detector if they were matched to an EM cluster.

Converted photons were identified using a modified version of the algorithm employed in the analysis of Standard Model muon pairs [28]. The tracks and clusters associated with the conversion were combined into a single four-vector representing the photon.

A track was selected as an electron candidate if it satisfied any of the following criteria: a loose cut on the output of the neural network described in Ref. [31]; $0.8 < E/p < 1.3$; or $0.5 < E/p < 2.0$ and the signed $\mathrm{d}E/\mathrm{d}x$ weight [34] was consistent with the track being an electron.

A track was selected as a muon candidate if it satisfied either the criteria employed in the analysis of Standard Model muon pairs [28], or the criteria employed in the analysis of inclusive

muons in multihadronic events given in Ref. [35], with no cut on the kaon signal $\mathrm{d}E/\mathrm{d}x$ weight.

Tau candidates were identified if they satisfied all of the following criteria: there was at least one and not more than three charged tracks within a cone of half-opening angle 35°; the invariant mass of all tracks within the cone was less than 1.2 GeV (assuming a pion mass for each track); and the invariant mass of all tracks and clusters within the cone was less than 2.0 GeV.

Electron and muon candidates were considered as isolated if the sum of the momenta of all additional charged particles within a cone of half-opening angle 20° centred on the track was less than 1.0 GeV, and the sum of the energy of additional clusters within the same cone was also less than 1.0 GeV. Tau candidates were considered as isolated if the sum of the momenta of charged particles within a cone of half-opening angle 60°, but outside the cone of half opening angle 35°, was less than 0.3 GeV and if the sum of the energy of clusters within the same region was also less than 0.3 GeV. If a track had been identified as an electron or muon candidate, but failed the relevant isolation cuts, then it was considered as a tau candidate if it satisfied the tau identification and isolation requirements given above.

A potential background to the search for lepton pairs with missing transverse momentum arises from Standard Model events containing neutrinos or poorly measured tracks. In such events the value of p_t^{miss} may be large and the missing momentum vector may point at a large angle to the beam direction; such events may thus escape cuts on these quantities. We defined the quantity a_t^{miss}, the component of p_t^{miss} that is perpendicular to the event thrust axis in the transverse plane. Since the Standard Model background events tend to be coplanar, this quantity is much less sensitive than p_t^{miss} to the presence of neutrinos or poorly measured particles. For events with a small acoplanarity angle between the lepton candidates, $\phi_{\mathrm{acop}} < 1.2$ rad, a cut on a_t^{miss} was applied and the direction of the missing momentum vector has been calculated (see 5(c) below) using a_t^{miss} rather than p_t^{miss}. These cuts give a sufficiently large reduction of the background that a hard cut on ϕ_{acop} is not needed and the cut on p_t^{miss} may be loosened, which increases the signal efficiency at low values of Δm. At large acoplanarity angle, $\phi_{\mathrm{acop}} \geq 1.2$ rad, a cut on a_t^{miss} no longer discriminates sufficiently between signal and background and more conventional cuts on p_t^{miss} and the direction of the missing momentum vector were applied.

The event selection cuts fall logically into three groups. The first set of cuts required evidence for the production of a pair of leptons, at least one of which must satisfy tight requirements on p_t, lepton identification, and isolation.

Events were retained if they satisfied the following cuts:

1. There was at least one isolated lepton candidate with $p_t > 1.5$ GeV.

2. If the event contained a second isolated lepton candidate, it was required that there be no other good tracks apart from the two lepton tracks. If any additional electromagnetic clusters were present then the measured acoplanarity angle and acollinearity angle between the two leptons were corrected by adding the four-momentum of the cluster to the lepton to which it was nearest in ϕ. The values $p_t^{\mathrm{miss}}/E_{\mathrm{beam}}$ and $a_t^{\mathrm{miss}}/E_{\mathrm{beam}}$ were also corrected for the presence of additional clusters.

3. If the event contained only one isolated lepton candidate then the tracks and clusters not associated with the lepton candidate were considered as a possible second lepton candidate if they satisfied the following requirements:

   (a) There was at least one additional good track with p_t greater than 0.3 GeV.

   (b) The total number of additional tracks and clusters was not greater than 4.

   (c) The invariant mass of the additional tracks and clusters did not exceed 1.0 GeV.

   If the event contained only one isolated lepton candidate and these requirements on the additional tracks and clusters were not satisfied, then the event was rejected.

4. In the search for $\tilde{e}^+\tilde{e}^-$ and $\tilde{\mu}^+\tilde{\mu}^-$ it was required that there was at least one isolated electron or muon candidate. In the search for $\tilde{\tau}^+\tilde{\tau}^-$ this requirement was not made.

The second set of event selection cuts required evidence for the production of an invisible system that carried away significant missing energy and momentum:

5. As discussed above, different cuts on the missing momentum and its direction were applied in the regions of small and large acoplanarity angle:

   small acoplanarity angle $\phi_{\rm acop} < 1.2$ rad:

   (a) $p_t^{\rm miss}/E_{\rm beam} > 0.035$;

   (b) $a_t^{\rm miss}/E_{\rm beam} > 0.025$;

   (c) $|\cos\theta_{\rm a}^{\rm miss}| < 0.95$, where the direction of the missing momentum vector was calculated using the missing momentum perpendicular to the event axis in the transverse plane, $\theta_{\rm a}^{\rm miss} = \tan^{-1}(a_t^{\rm miss}/p_{\rm z}^{\rm miss})$ and $-p_{\rm z}^{\rm miss}$ is the total momentum of the observed particles in the z direction.

   large acoplanarity angle $\phi_{\rm acop} \geq 1.2$ rad:

   (d) $p_t^{\rm miss}/E_{\rm beam} > 0.045$;

   (e) $|\cos\theta_{\rm p}^{\rm miss}| < 0.90$, where the direction of the missing momentum vector is given by $\theta_{\rm p}^{\rm miss} = \tan^{-1}(p_t^{\rm miss}/p_{\rm z}^{\rm miss})$.

6. The acollinearity angle was greater than 0.3 rad.

The remaining event selection cuts reduced the likelihood that the signature of missing momentum could have been faked by background processes:

7. Events with clusters of more than 1 GeV in SW or FD (including the gamma-catcher) were rejected. Low energy clusters were required to be back-to-back with the observed system of central detector tracks and electromagnetic clusters. This is in order to reduce the sensitivity to random low energy clusters caused by possible detector noise or off-momentum electrons. If there was only one FD or SW cluster and it had a scaled energy $x_{\rm FDSW} = E/E_{\rm beam} < 0.4$ the event was rejected if $\Delta\phi_{\rm FDSW} < 1$ rad, where $\Delta\phi_{\rm FDSW}$ is the acoplanarity angle between the SW–FD cluster and the total momentum vector of the observed tracks and electromagnetic clusters.

8. Events containing high energy isolated photons were rejected. To be considered isolated, it was required that there be no other electromagnetic clusters or tracks within a cone of half angle 20° around the photon direction. The energy threshold was 2 GeV in the regions $0.71 < |\cos\theta| < 0.83$ and $|\cos\theta| > 0.965$, in which the resolution of the calorimeter is degraded due to upstream material or poor containment. The energy threshold was 6 GeV elsewhere.

9. To reject backgrounds from beam-gas or beam-wall collisions, the number of good tracks divided by the total number of tracks was required to be greater than 0.2.

10. A particularly difficult potential background originates from $e^+e^-\mu^+\mu^-$ events in which one of the electrons and one of the muons is observed and the second muon is scattered at an angle to the beam direction of less than about $\cos^{-1}(0.965)$. Below this angle a muon can carry away a significant $p_t^{\rm miss}$ and may thus cause the event to be selected. To reduce the potential background from this source, events were rejected if: a track with $|\cos\theta| > 0.96$ was reconstructed in the central detector (but failed the standard quality criteria) or in the muon detector or hadron calorimeter that satisfied $\Delta\phi < 1$ rad, where $\Delta\phi$ is the acoplanarity angle between the track and the total momentum vector of the observed good tracks and electromagnetic cluster.

11. Events were rejected if the lepton candidates had the same electric charge.

12. The acoplanarity angle, without the correction for additional electromagnetic clusters, was required to be greater than 0.1 rad. This cut removed events in which the lepton pair was perfectly coplanar; the non-zero $p_t^{\rm miss}/E_{\rm beam}$ therefore arises from electromagnetic clusters not associated with the leptons.

No events in the data survived the above selection. A number of cuts (2, 3b, 3c, 4, 5a, 6, 8–12) exclusively remove no candidate events in the data. That is, if any one of these cuts were removed there would still be no selected events in the OPAL data.

In the search for selectron and smuon pairs, the total background predicted by the Standard Model Monte Carlo simulation was 0.6 events. A breakdown into the contributions from individual background processes is given in the last row of Table 2. As can be seen from Table 2, the dominant expected background remaining after the event selection cuts arises from four-fermion final states (0.42 events). In the search for $\tilde{\tau}^+\tilde{\tau}^-$ events, cut 4 was not applied, and a total background of 1.1 events is expected.

Figure 2 shows the distribution of the variables used in cut 5 (missing momentum and its direction). To examine the background events that lie just outside the region defined as the signal acceptance, each distribution is shown after a loose selection (dropping cuts 2, 6, 9, and 10, and relaxing the requirements listed in 3 and 5) has been applied.

Table 3 gives some typical selection efficiencies for $\tilde{e}^+\tilde{e}^-$, $\tilde{\mu}^+\tilde{\mu}^-$ and $\tilde{\tau}^+\tilde{\tau}^-$ production.

	Data	Total Backg.	$f\bar{f}(\gamma)$	$e^+e^-f\bar{f}$	4-f	$\tilde{\mu}^+\tilde{\mu}^-$(%)
cut (1)	20120	19829.4	9486.9	10339.9	2.5	99.6
cuts (2),(3),(4)	4787	5443.6	2134.2	3308.6	0.6	90.2
cut (5)	192	221.6	9.5	211.5	0.5	71.8
cut (6)	189	213.2	1.9	210.8	0.5	71.8
cut (7)	1	3.0	1.6	0.9	0.5	71.4
cut (8)	0	1.4	0.1	0.9	0.4	71.0
cut (9)	0	1.4	0.1	0.9	0.4	71.0
cut (10)	0	1.1	0.1	0.6	0.4	71.0
cut (11)	0	0.7	0.1	0.2	0.4	70.9
cut (12)	0	0.6	0.0	0.2	0.4	70.9

Table 2: *Analysis B: The remaining numbers of events normalised to the integrated luminosity of the data for various Monte Carlo background processes are compared with data (first column) after each cut. Efficiencies for a simulated event sample of $\tilde{\mu}^+\tilde{\mu}^-$ are also given for $m_{\tilde{\mu}}$=60 GeV and Δm=5 GeV.*

		$\tilde{e}^+\tilde{e}^-$	$\tilde{\mu}^+\tilde{\mu}^-$	$\tilde{\tau}^+\tilde{\tau}^-$
$m_{\tilde{\ell}}$ (GeV)	Δm (GeV)	Efficiency (%)	Efficiency (%)	Efficiency (%)
50	2	31.8±1.5	32.8±1.5	0.1±0.1
50	5	63.3±1.5	67.0±1.5	12.8±1.1
50	10	66.0±1.5	72.1±1.4	25.6±1.4
50	$m_{\tilde{\ell}^\pm}/2$	68.1±1.5	72.6±1.4	33.6±1.5
50	$m_{\tilde{\ell}^\pm}$	65.9±1.5	72.3±1.4	34.6±1.5
65	2	23.2±1.3	20.7±1.3	0.0±0.0
65	5	65.0±1.5	71.2±1.4	10.8±1.0
65	10	72.3±1.5	76.4±1.4	25.8±1.0
65	$m_{\tilde{\ell}^\pm}/2$	71.7±1.4	77.2±1.3	42.0±1.6
65	$m_{\tilde{\ell}^\pm}$	72.0±1.4	76.7±1.3	40.2±1.6

Table 3: *Analysis B: Detection efficiencies in percent for slepton pair production using samples of 1000 simulated events for two different selectron, smuon, and stau masses and five different $\Delta m = (m_{\tilde{\ell}^\pm} - m_{\tilde{\chi}_1^0})$ values. The errors are due to Monte Carlo statistics only.*

4.3 Systematic errors

The systematic errors that have been considered on the number of expected events were estimated as follows:

1. The statistical error of the $\tilde{\ell}^{\pm}$ Monte Carlo simulation.

2. The systematic error on the integrated luminosity is 0.9% [4], which is evaluated from half the difference $(1.8 \pm 1.3)\%$ between the luminosities measured by the FD detector and the SW detector.

3. The systematic error due to trigger efficiency is estimated to be negligible because of the track transverse momentum requirement.

4. The inefficiency of the veto on SW–FD clusters (cut 7 of Analysis B) caused by beam-related backgrounds or detector noise (which is not simulated in the Monte Carlo) was estimated from a study of randomly triggered beam crossings to be 0.6%.

5. The accuracy with which the Monte Carlo simulates the lepton identification has been checked using $e^+e^-e^+e^-$ and $e^+e^-\mu^+\mu^-$ events. The muon identification efficiency was found to be equal in data and Monte Carlo to within the 0.7% statistical accuracy of the check. The electron identification efficiency was found to be lower in data than the Monte Carlo by $(2 \pm 1)\%$. If the lepton identification efficiency is reduced by 2% the slepton pair event selection efficiency for Analysis B is reduced by about 0.3% which is taken as a systematic error.

6. The systematic uncertainty due to different angular distributions (possible for selectron pair production via the t-channel) of produced sleptons and decay products was estimated for six different MSSM parameter sets, representing different neutralino masses and couplings. Differences in selection efficiencies were found to be at the level of 1%.

The systematic errors were considered to be independent, and the total systematic error was calculated as a quadratic sum of the individual errors. In computing the limits, the number of expected events was reduced by the total systematic error.

4.4 Results

No events were selected as charged slepton pair candidates in either Analysis A or Analysis B. The latter analysis has a higher expected sensitivity and was used for setting limits on slepton pair production. Two approaches were considered. In the first one, upper limits on the cross-sections as a function of slepton and $\tilde{\chi}_1^0$ masses were calculated in a model independent way. In the second one, limits on the slepton masses were calculated in the framework of the MSSM.

The number of events which would be selected has been calculated as a function of $m_{\tilde{\ell}^{\pm}}$ and $m_{\tilde{\chi}_1^0}$. The efficiency at any arbitrary point in the $(m_{\tilde{\ell}^{\pm}},\ m_{\tilde{\chi}_1^0})$ plane was obtained by a two-dimensional linear interpolation between the efficiencies determined using Monte Carlo

simulations. The upper limits on the production cross-section at the 95% C.L. for $\tilde{\ell}^+\tilde{\ell}^-$ are shown in Fig. 3a-c. The cross-section limits have been computed taking into account, at each centre-of-mass energy, the integrated luminosity, the expected production cross-section and the estimated detection efficiency. These limits do not depend on the details of SUSY models, except for the assumptions that the $\tilde{\chi}_1^0$ is the lightest supersymmetric particle and that the $\tilde{\chi}_1^\pm$ and $\tilde{\chi}_2^0$ are heavier than the sleptons. Alternatively, these results may be interpreted as placing limits on the product $\sigma \cdot \mathrm{Br}^2$, where σ is the production cross-section for $\tilde{\ell}^+\tilde{\ell}^-$ and Br is the branching ratio for the decay $\tilde{\ell}^\pm \to \ell^\pm + \tilde{\chi}_1^0$.

Since in constrained (i.e., common m_0 value at the GUT scale) MSSM models, right-handed sleptons are always lighter than their left-handed partners and the cross-section for production of right-handed sleptons is usually smaller than that for left-handed ones, the MSSM mass limits were conservatively calculated using cross-sections corresponding to right-handed slepton production. In this framework, the predicted cross-sections for $\tilde{\mu}$ and $\tilde{\tau}$ production are of the order of 0.1–0.2 pb for a heavy ($m_{\tilde{\ell}} > 50$ GeV) $\tilde{\mu}$ and $\tilde{\tau}$. In the MSSM framework, the available luminosity delivered at $\sqrt{s} = 130 - 136$ GeV at LEP therefore does not provide sensitivity to larger masses than are already excluded at LEP running on the Z^0 peak (LEP 1) [36].

The production cross-section for $\tilde{\mathrm{e}}$ can be enhanced by the presence of the t-channel neutralino exchange, especially for $|\mu| \gg M_2$ (gaugino region). Figure 3d shows the 95% C.L. exclusion limits for right-handed selectrons, for $\mu = -200$ GeV and $\tan\beta = 1.5$. With the available luminosity, the complete MSSM parameter space that is kinematically accessible cannot be excluded. A typical point of parameter space where the selectron production cross-sections are enhanced (without being the most favourable case) has been chosen. In the case of a massless $\tilde{\chi}_1^0$, a right-handed selectron with a mass lighter than 58.0 GeV is excluded at the 95% C.L. Taking into account the OPAL present mass limit on $\tilde{\chi}_1^0$ for the MSSM parameters considered [4], a 95% C.L. lower limit on the selectron mass of 57.2 GeV is derived for $m_{\tilde{\chi}_1^0} = 12.0$ GeV. These limits are obtained using the MSSM prediction for $\mathrm{Br}(\tilde{\mathrm{e}}_R \to \tilde{\chi}_1^0\mathrm{e})$ and assuming that the cascade decay $\tilde{\mathrm{e}}_R \to \tilde{\chi}_2^0\mathrm{e} \to \tilde{\chi}_1^0\mathrm{e}X$ (where $X = f\overline{f}, \gamma$ or h^0) is undetected. These limits are valid for all values of $|\mu| > 200$ GeV and $\tan\beta > 1.5$ since for increasing values of these parameters, the corresponding selectron production cross-section also increases. For the chosen values of μ and $\tan\beta$, the excluded region of Fig. 3d corresponds to $M_2 < 80$ GeV.

5 Search for semileptonically decaying charginos

If charginos are pair-produced in $\mathrm{e}^+\mathrm{e}^-$ collisions and then both decay semileptonically with final decay products $\tilde{\chi}_1^\pm \to \tilde{\chi}_1^0\ell^\pm\nu$ (via intermediate virtual W's, real or virtual $\tilde{\ell}$'s, or real or virtual $\tilde{\nu}$'s, including interference effects), the event topology would be that of an acoplanar pair of leptons and missing energy, very similar to the one produced by slepton decays presented in the previous section. Although the chargino is usually expected to decay into $\tilde{\chi}_1^\pm \to \tilde{\chi}_1^0\mathrm{W}^*$ with a large hadronic branching fraction over most of MSSM parameter space, large semileptonic branching ratios for the chargino could be expected for small values of m_0 leading to light sleptons and sneutrinos. Analysis B described in subsection 4.2 has been used to search for semileptonic decays of charginos.

The efficiencies obtained for various $m_{\tilde{\chi}_1^+}$ and $\Delta m = (m_{\tilde{\chi}_1^+} - m_{\tilde{\chi}_1^0})$ values are shown in

Table 4. The same treatment for the systematic errors was used as outlined in subsection 4.3.

Δm	$m_{\tilde{\chi}_1^\pm}$ (GeV)				
(GeV)	45	50	55	60	65
2	1.1 ± 0.3	1.5 ± 0.4	0.4 ± 0.2	0.4 ± 0.2	0.2 ± 0.1
5	14.6 ± 1.1	18.4 ± 1.2	19.4 ± 1.3	22.8 ± 1.3	21.4 ± 1.3
10	25.6 ± 1.4	32.8 ± 1.5	36.3 ± 1.5	39.1 ± 1.5	43.8 ± 1.6
$m_{\tilde{\chi}_1^+}/2$	21.8 ± 1.3	40.3 ± 1.6	44.0 ± 1.6	52.9 ± 1.6	57.6 ± 1.6
$m_{\tilde{\chi}_1^+}$	24.3 ± 1.4	41.5 ± 1.6	49.1 ± 1.6	54.7 ± 1.6	60.8 ± 1.5

Table 4: *Chargino analysis: Selection efficiencies in percent for $\tilde{\chi}_1^+\tilde{\chi}_1^-$ production using five different values of $m_{\tilde{\chi}_1^\pm}$ and five different values of $\Delta m = (m_{\tilde{\chi}_1^+} - m_{\tilde{\chi}_1^0})$. The errors are statistical only.*

No evidence for chargino decays has been observed. We have computed 95% C.L. upper limits on the production cross-section for charginos, under the assumption of a 100% branching ratio to $\tilde{\chi}_1^\pm \to \tilde{\chi}_1^0 \ell^\pm \nu$. These limits are shown in Fig. 4. They improve on the $\tilde{\chi}_1^\pm \to \tilde{\chi}_1^0 \ell^\pm \nu$ model independent limits in a previous publication [4], especially in the region of small Δm. Again, these results may be interpreted as placing limits on the product $\sigma \cdot \mathrm{Br}^2$, where here σ is the production cross-section for $\tilde{\chi}_1^+\tilde{\chi}_1^-$ and Br is the branching ratio for the decay $\tilde{\chi}_1^\pm \to \tilde{\chi}_1^0 \ell^\pm \nu$.

6 Search for scalar top (stop) quarks

If the stop quark is assumed to be the lightest charged sparticle, the dominant decay mode would be $\tilde{t}_1 \to c + \tilde{\chi}_1^0$. The experimental signature for $\tilde{t}_1\bar{\tilde{t}}_1$ events would therefore be an acoplanar two-jet topology with large transverse momentum with respect to the beam axis. This signature resembles that produced by chargino hadronic decays. Consequently this analysis is similar to the one described in Ref. [4], apart from a different optimisation of the cuts. The data sample used for the stop search consisted of 2.6 pb^{-1} at $\sqrt{s} = 130$ GeV and 2.6 pb^{-1} at $\sqrt{s} = 136$ GeV.

If the two jets are very close to each other, the event signature is a monojet topology. Such monojet events were also selected to obtain high detection efficiency. If the mass difference between $\tilde{t}_1$ and $\tilde{\chi}_1^0$ is smaller than 5 GeV, the visible energy and the transverse momentum also become small. The selection was designed to maintain reasonable efficiency down to this small mass difference region, because a stop quark lighter than 90 GeV has already been excluded [9] if the mass difference is larger than 35 GeV.

The selection cuts are listed below and the numbers of events remaining after each cut are given in Table 5. For comparison, the table also shows the corresponding numbers for the simulated background processes and a sample of simulated $\tilde{t}_1\bar{\tilde{t}}_1$ events. The distributions of the cut variables are well modelled by Monte Carlo as was shown in Ref. [4].

1. The number of charged particle tracks was required to be at least four, and the ratio of the number of good tracks to the total number of tracks was required to be greater than 0.2 to eliminate beam-gas and beam-wall backgrounds.

2. To reduce the background from two-photon processes and multihadronic events where a jet axis was close to the beam direction, the total energy deposited in each silicon tungsten calorimeter had to be less than 5 GeV, less than 2 GeV in each forward calorimeter, and less than 5 GeV in each gamma-catcher. In addition, the visible energy in the region of $|\cos\theta| > 0.8$ was required to be less than 30% of the total visible energy.

3. Events with small missing transverse momentum were eliminated by demanding that the missing transverse momentum of the event excluding the hadron calorimeter, $p_t^{\rm miss}$, be greater than 4 GeV and that the missing transverse momentum including hadron calorimeter information, $p_{t,\rm HCAL}^{\rm miss}$, be greater than 5 GeV. Although most of the events from two-photon processes were rejected by the $p_t^{\rm miss}$ cut, the $p_{t,\rm HCAL}^{\rm miss}$ cut was applied to reject occasional two-photon events with a high transverse momentum neutral hadron.

4. Events from the process $\rm e^+e^- \to Z\gamma$ where the γ escaped along the beam pipe were rejected by requiring that the polar angle of the missing momentum direction, $\theta_{\rm miss}$, satisfied $|\cos\theta_{\rm miss}| < 0.8$.

5. To remove a large fraction of the multihadron events, the visible energy was required to be less than $0.5\sqrt{s}$.

6. Events that were kinematically consistent with $\tau^+\tau^-(\gamma)$ were rejected as described in Ref. [4].

7. The events were then divided into two hemispheres by the plane perpendicular to the thrust axis. If one of the hemispheres had an energy of less than 1 GeV and also contained no good tracks, the event was categorised as a monojet event. Otherwise the event was classified as a dijet event. According to these criteria, after cut (6) one event in the data was classified as a dijet event, and no event as a monojet event.

D1. For dijet events, the acoplanarity angle $\phi_{\rm acop}$ between the momentum sums in the two hemispheres was required to be greater than 15°.

M1. For events classified as monojets, to reject the four-fermion process $\rm e^+e^- \to Z^*\gamma^* \to \nu\bar{\nu}q\bar{q}$ the thrust value of the event was required to be smaller than 0.96. Because this $\rm q\bar{q}$ pair is emitted from the γ^*, the invariant mass of the $\rm q\bar{q}$ system is small and the thrust is expected to be close to unity.

No events were observed in the data after the above cuts. The efficiency for $\tilde{\rm t}_1\bar{\tilde{\rm t}}_1$ events was above 50% for $m_{\tilde{\rm t}_1} = 55$ GeV and $m_{\tilde{\chi}_1^0} = 45$ GeV. Some typical efficiency values are listed in Table 6. A high efficiency value of about 35% was obtained for the small mass difference of $\Delta m (= m_{\tilde{\rm t}_1} - m_{\tilde{\chi}_1^0}) = 5$ GeV.

For the extraction of limits described in the following section the efficiency at an arbitrary point of $m_{\tilde{\rm t}_1}$ and $m_{\tilde{\chi}_1^0}$ was interpolated using a polynomial fit to the efficiencies determined using Monte Carlo simulations.

6.1 Systematic errors

The systematic errors on the number of expected events are summarised as follows:

	Data	Total Backg.	$q\bar{q}(\gamma)$	$\tau\tau(\gamma)$	$e^+e^-f\bar{f}$	4-f	$\tilde{t}_1\bar{\tilde{t}}_1$ (%)
$m_{\tilde{t}_1}$ (GeV)							55
$m_{\tilde{\chi}^0_1}$ (GeV)							45
no cuts	–	–	1650	110	105k	11.1	100.0
cut (1)	26371	30874	1601	30.6	29.2k	1.87	93.4
cut (2)	4750	4501	765	18.3	3717	0.98	73.7
cut (3)	436	439	420	14.3	3.4	0.95	62.6
cut (4)	227	249	235	11.7	1.6	0.92	57.9
cut (5)	4	7.10	0.94	3.97	1.6	0.59	57.9
cut (6)	1	4.13	0.94	1.00	1.6	0.59	57.8
dijet	1	3.69	0.94	0.99	1.6	0.16	48.0
cut (D1)	0	0.54	0.05	0.09	0.26	0.14	43.6
monojet	0	0.44	0.0	0.01	0.00	0.43	9.8
cut (M1)	0	0.16	0.0	0.01	0.00	0.15	9.4
(D1+M1)	0	0.70	0.05	0.10	0.26	0.29	53.0

Table 5: *Stop analysis: The remaining numbers of events normalised to the integrated luminosity of the data for various background processes are compared with data after each cut. Efficiencies for a simulated event sample of $\tilde{t}_1\bar{\tilde{t}}_1$ are also given. The numbers given after cut (D1) are for dijet events only, and the numbers after cut (M1) are for monojet events only. The numbers of events expected from two-photon processes do not include the region $m_{\gamma\gamma} < 3$ GeV with $Q^2 < 1.3$ GeV^2.*

1. Statistical error of the $\tilde{t}_1$ Monte Carlo simulation.

2. The systematic error on the integrated luminosity was 0.9%.

3. The systematic error due to trigger efficiency was estimated to be negligible after the requirement of at least four good tracks.

4. Fragmentation function for $\tilde{t}_1$: The multiplicity and the visible energy of the $\tilde{t}_1\bar{\tilde{t}}_1$ events depend on the fragmentation function of the $\tilde{t}_1$. The fragmentation scheme proposed by Peterson et al. [37] was used, in which the fragmentation parameter $\epsilon_{\tilde{t}_1}$ was rescaled (using the top to bottom quark mass ratio) from the fragmentation parameter measured for the bottom quark [38]. The systematic uncertainty due to this parameter was estimated to be 3%.

   We have also used the fragmentation function proposed by Bowler [39] instead of the Peterson function, because the shape of this fragmentation function is very different from that of Peterson. The systematic error, based on the difference of the two fragmentation functions, was typically 1–2%, which was smaller than that due to the variation of the $\epsilon_{\tilde{t}_1}$ parameter using the Peterson fragmentation function alone. This 2% error was added quadratically to the systematic error due to the $\tilde{t}_1$ fragmentation.

5. Fragmentation of the charm quark: The charm quark and the spectator quark were also fragmented, and the systematic error due to the uncertainty in charm quark fragmentation was estimated to be typically 2%.

Δm	$m_{\tilde{t}_1}$ (GeV)	
(GeV)	50	60
3	12.0 ± 1.0	6.7 ± 0.8
5	38.5 ± 1.5	35.8 ± 1.5
10	53.0 ± 1.6	53.2 ± 1.6
20	53.6 ± 1.6	53.1 ± 1.6
30	45.4 ± 1.6	48.5 ± 1.6
40	32.8 ± 1.5	39.1 ± 1.5
$m_{\tilde{t}_1}$	30.8 ± 1.5	30.3 ± 1.4

Table 6: *Stop analysis: Selection efficiencies in percent for $\tilde{t}_1\bar{\tilde{t}}_1$ production using samples of 1000 events for two different values of $m_{\tilde{t}_1}$ and for seven different values of $\Delta m = (m_{\tilde{t}_1} - m_{\tilde{\chi}_1^0})$. The errors are statistical only.*

The systematic errors were considered to be independent, and the total systematic error was calculated as a quadratic sum of the individual errors. The number of expected events was reduced by the total systematic error.

6.2 Results

No evidence for stop quark pair production was observed in the data. The absence of observed events was consistent with the expected background of 0.7 events. Figure 5 shows the excluded regions at 95% C.L. in the $(\theta_{\rm mix}, m_{\tilde{t}_1})$ plane for (a) a mass difference of $\Delta m (= m_{\tilde{t}_1} - m_{\tilde{\chi}_1^0}) \geq$ 5 GeV and (b) $10 \leq \Delta m \leq 20$ GeV.

Numerical mass bounds are listed in Table 7 for various values of $\theta_{\rm mix}$. Assuming that Δm is greater than 5 GeV and that $\tilde{t}_1$ is purely left-handed ($\theta_{\rm mix} = 0$), $\tilde{t}_1$ must be heavier than 52.4 GeV. For $\theta_{\rm mix} \leq \frac{\pi}{8}$, $\tilde{t}_1$ must be heavier than 49.4 GeV.

Excluded $m_{\tilde{t}_1}$ region (GeV)		
$\theta_{\rm mix}$ (rad)	$\Delta m \geq 5$ GeV	$10 \leq \Delta m \leq 20$ GeV
0.0	≤ 52.4	≤ 55.5
$\leq \frac{\pi}{8}$	≤ 49.4	≤ 53.0
$\leq \frac{\pi}{4}$	$\leq 45.5^*$	$\leq 46.0^*$
0.98	$\leq 43.0^*$	$\leq 44.5^*$

Table 7: *The excluded $m_{\tilde{t}_1}$ region ($\Delta m = m_{\tilde{t}_1} - m_{\tilde{\chi}_1^0}$) at 95% C.L. The numbers with a star show the previous limits obtained at LEP running at the Z^0 peak [40].*

7 Particles decaying to four-jet final states

7.1 Introduction

We have performed a search for the associated production of two massive particles, X and Y, via the process $e^+e^- \to XY$, where we assume that both X and Y decay into a $q\overline{q}$ pair. We have therefore searched for jet-jet mass resonances in the four-jet final state. The data sample used for this search consisted of 2.6 pb^{-1} at $\sqrt{s} = 130$ GeV and 2.6 pb^{-1} at $\sqrt{s} = 136$ GeV.

The process $e^+e^- \to A^0h^0$, where A^0 and h^0 are Higgs bosons predicted by models beyond the Standard Model that contain at least two Higgs doublets, is one example of the reaction $e^+e^- \to XY$. The total integrated luminosity collected at 130 and 136 GeV is too low to improve the mass limits of the previous OPAL search [41] for A^0 and h^0 at LEP1. In the mass region of interest the cross-section predicted by the MSSM is 0.1 pb or less for accessible values of the model parameters; therefore, the present search for the process $e^+e^- \to XY \to$ four jets is to be considered in a more general, model independent context.

7.2 Analysis

Multihadronic events were first selected [42]. The energies and momenta of jets were recalculated using the global corrected energy flow (GCE) [29] algorithm to combine tracks, electromagnetic and hadron calorimeter clusters. The following selection criteria were then applied:

1. To reduce "radiative return" $e^+e^- \to Z\gamma$ events, we calculated $\sqrt{s'}$, the effective centre-of-mass energy, by performing a kinematic fit to determine the energy of any unmeasured photon along the beam direction, or by using the energy of an isolated photon observed in the detector. The reconstructed $\sqrt{s'/s}$ distribution is shown in Fig. 6a. We selected non-radiative events by demanding $s'/s \geq 0.8$.

2. Jets were reconstructed and the thrust axis determined using charged particle tracks, electromagnetic and hadron calorimeter clusters. In Fig. 6b the distribution of $\log_{10} y_{34}$ is shown for the non-radiative events, where y_{34} is the value of $y_{\rm cut}$ at which events change from three to four jets in the Durham jet-finding scheme [43]. Events with four or more jets were selected by requiring $y_{34} \geq 0.01$.

3. Finally the event sphericity was required to be greater than 0.2. The sphericity distributions before and after the y_{34} selection are plotted in Fig. 6c and 6d, respectively.

As indicated in Table 8, 17 events passed the criteria above, whereas the expected number from the $q\bar{q}(\gamma)$ Monte Carlo sample is 10.4 ± 0.8 and the expected number from four-fermion processes, simulated with the EXCALIBUR [26] Monte Carlo, is 0.8 ± 0.1 events. The data show some excess compared to the $q\bar{q}(\gamma)$ Monte Carlo expectation particularly after applying the final cut (see Fig. 6d); however, the excess is not significant.

The signal efficiencies for A^0h^0 production with $m_{A^0} \simeq m_{h^0} \simeq 55$ GeV are listed in Table 8, together with the number of data events and the background estimate from $q\bar{q}(\gamma)$ and four-fermion events.

The events were then forced to contain exactly four jets, and the invariant masses of pairs of jets were reconstructed. A kinematic fit was performed imposing energy and momentum conservation constraints to improve the jet-jet mass resolution. There are three possible ways of combining the four jets into pairs; these can be ordered according to the difference between the two reconstructed masses. If the mass difference between the A^0 and h^0 is 10 GeV or less, the pairing with the minimum difference between the two reconstructed masses has the highest probability of arising from the A^0 and h^0. In this case, the peak of the summed reconstructed masses reproduces the sum of the input values to within 0.5 GeV, and the expected mass resolution is about 2 GeV. The distribution of the sum of the two jet-jet invariant masses for the combination with the smallest difference between the two masses after all selection cuts is shown in Fig. 7a.

Cut	Data	$q\bar{q}(\gamma)$	4-f	Sig. Efficiency (%)
Multihadron selection	1583	1502.2 ± 9.4	10.8 ± 0.2	100.0
$s'/s \geq 0.8$	353	382.8 ± 4.7	5.1 ± 0.2	87.8 ± 0.7
$y_{34} \geq 0.01$	20	17.4 ± 1.0	1.0 ± 0.1	58.2 ± 0.9
$S \geq 0.2$	17	10.4 ± 0.8	0.8 ± 0.1	54.0 ± 0.8
Loose b-tagging (see text)	3	0.9 ± 0.2	0.10 ± 0.02	38.1 ± 1.0
Tight b-tagging (see text)	0	0.5 ± 0.2	0.04 ± 0.01	28.7 ± 1.0

Table 8: *Four-jet analysis: The numbers of events detected after each cut is applied. The expected numbers of background events from the* $q\bar{q}(\gamma)$ *and four-fermion Monte Carlo samples and the expected detection efficiencies for the signal are also given. The Monte Carlo signal sample is* $e^+e^- \rightarrow A^0h^0$ *where both* A^0 *and* h^0 *decay into* $b\bar{b}$ *for the case* $m_{A^0} \simeq m_{h^0} \simeq 55$ *GeV. The errors are from Monte Carlo statistics only.*

For the specific case of A^0h^0 production a clear signature of four b-quarks is expected, since the branching ratio of both A^0 and h^0 to $b\bar{b}$ is predicted to be about 90%. The b-tagging is applied with the same algorithm as in the measurement of the $Z^0 \rightarrow b\bar{b}$ branching fraction [44]. By requiring at least one jet with a secondary vertex of decay length significance [44] $L/\sigma_L > 4.0$ (loose b-tagging) 3 events remain in the final data sample, which is consistent with the number of expected background events of 1.0 ± 0.2. The signal efficiency for A^0h^0 is about 38%. Additionally requiring a second vertex with $L/\sigma_L > 2$ or a high p_t lepton (tight b-tagging) removes all events, while the total efficiency for the A^0h^0 signal at this stage is expected to be still about 29%. This clearly disfavours a large contribution of $A^0h^0 \rightarrow b\bar{b}b\bar{b}$ production.

Recently the ALEPH collaboration has reported an excess of four-jet events and an enhancement in the sum of the two jet-jet masses around 105 GeV [1] with a reported cross-section of 3.1 ± 1.7 pb under a particle pair hypothesis. We do not observe such an effect in Fig. 7a. We therefore also present an analysis that closely follows the selection of Ref. [1] to check that a possible signal is not being lost.

Starting from our inclusive multihadron sample we applied the following selection cuts:

1. The total visible mass, $m_{\rm vis}$, and the absolute value of the momentum along the beam direction, $|p_z^{\rm vis}|$, were required to satisfy $|p_z^{\rm vis}| \leq 0.75 \cdot (m_{\rm vis} - 90.0\,{\rm GeV})$.

2. To select four-jet events we required $y_{34} \geq 0.008$.

3. All jets were required to satisfy $E_{\rm had}/E_{\rm jet} = (E_{\rm CT} + E_{\rm HCAL})/(E_{\rm CT} + E_{\rm HCAL} + E_{\rm EM}) \geq 0.2$, where $E_{\rm CT}$, $E_{\rm EM}$ and $E_{\rm HCAL}$ are the energies of charged particles, electromagnetic clusters and hadron clusters, respectively.

4. Each of the four jets was required to have a jet mass of at least 1.0 GeV.

5. A kinematic fit was performed on the four-jet final state imposing the four constraints of energy and momentum conservation.

6. All combinations of jet-jet masses were required to exceed $m_{ij} \geq 25$ GeV.

7. The sum of the masses of all pairs of jets had to satisfy $(m_i + m_j) \geq 10$ GeV.

8. All combinations of two jets were required to have a total of at least 10 charged particle tracks.

Seven events pass these criteria (no b-tagging was required), compared with an expected $\rm q\bar{q}(\gamma)$ background of 6.4 ± 0.6 events and expected four-fermion background of 0.25 ± 0.03 events. The efficiency of this analysis is $(40.5 \pm 0.7)\%$ for $\rm A^0h^0$ production, comparable with the efficiency of 42.0% and expected background from Standard Model processes of 8.6 ± 0.3 events in the ALEPH analysis [1] using an integrated luminosity of 5.7 $\rm pb^{-1}$. The distribution of the sum of the two jet-jet masses for the minimum mass difference combination is shown in Fig. 7b. We do not observe any excess of events in the region around 105 GeV.

7.3 Upper limits on the production cross-section

No significant peak is seen in the sum of the jet-jet mass distribution for four-jet events. The first set of selection criteria is used to compute upper limits on the production cross-section for $\rm e^+e^- \to XY$. These have been calculated using signal efficiencies derived from the $\rm e^+e^- \to A^0h^0$ Monte Carlo, with $m_{\rm A^0} \simeq m_{\rm h^0}$ and both $\rm A^0$ and $\rm h^0$ decaying to $\rm b\bar{b}$ quark pairs, but without requiring b-tagging. The angular distribution for $\rm A^0h^0$ production is $\rm d\sigma/dcos\theta \sim \sin^2\theta$, which is valid for the production of any two scalar particles in the s-channel. In evaluating the limits as a function of the sum of the jet-jet mass $(m_{\rm X} + m_{\rm Y})$, we selected events in a window of ± 4 GeV around a given dijet mass and scanned the mass spectrum in steps of 0.1 GeV. The expected sensitivity of the search, assuming a small ($\ll 1$ GeV) natural width for particles X and Y, showed little dependence on the size of the mass window provided it was greater than ± 3 GeV. The signal efficiency after the mass window requirement is $(28.3 \pm 0.6)\%$ for $(m_{\rm X} + m_{\rm Y}) \simeq 110$ GeV. The efficiency shows little variation with $(m_{\rm X} + m_{\rm Y})$ in the interval from 95 to 120 GeV. For $|m_{\rm X} - m_{\rm Y}| \leq 10$ GeV, the efficiency is reduced by at most 25% with respect to the equal mass case. The following systematic errors were considered when evaluating the upper limits:

1. Uncertainty on the integrated luminosity (0.9%) and from Monte Carlo statistics. The numbers of expected events were reduced by these uncertainties to set the upper limit.

2. Peak mass shift. The peak position in the mass distribution for the Monte Carlo simulation of h^0A^0 signal events shows no mass shift within an accuracy of 0.5 GeV. The mass window was moved within ± 0.5 GeV and the maximum number of events found was used to set the limit.

3. Error due to background expectation. The expected number of background events from the simulation was reduced by 20% to calculate the upper limit. This uncertainty reflects the statistical precision with which the four-jet rate arising from QCD processes has been tested at the present energies [45].

The upper limits obtained for the production cross-section for $m_X \simeq m_Y$ are shown in Fig. 8 as a function of the sum of the masses of X and Y.

8 Summary and Conclusions

We have searched for the pair production of several particles predicted by supersymmetric theories in a data sample corresponding to an integrated luminosity of more than 5 pb^{-1} at $\sqrt{s}$ =130–136 GeV collected with the OPAL detector. No evidence for production of any of these particles is observed.

In the search for charged sleptons no data events were observed satisfying all the requirements, compatible with the estimated number of 0.6 background events expected in the search for selectrons and smuons and 1.1 events in the search for staus. We have computed 95% C.L. upper limits for the production cross-section of the three types of sleptons. When considering the present lower mass limit on $\tilde{\chi}_1^0$ [4] for the MSSM parameters $\mu = -200$ GeV and $\tan\beta = 1.5$, a 95% C.L. lower limit on the right-handed selectron mass of 57.2 GeV is derived for $m_{\tilde{\chi}_1^0} = 12.0$ GeV. This limit is valid for all values of $|\mu| > 200$ GeV and $\tan\beta > 1.5$ and corresponds to $M_2 < 80$ GeV.

Pair-produced charginos, with both charginos decaying semileptonically, have been searched for using the same analysis. We have improved the $\tilde{\chi}_1^{\pm} \rightarrow \tilde{\chi}_1^0 \ell^{\pm} \nu$ model independent cross-section limits obtained in a previous publication [4].

In the search for stop quarks no data events were observed satisfying the selection criteria, compatible with the estimated 0.7 events expected from background sources. Mass bounds have been improved compared to the limits obtained at LEP running at the Z^0 peak.

We have searched for the associated production of two massive particles XY (i.e., $e^+e^- \rightarrow XY$, such as $e^+e^- \rightarrow h^0A^0$) both decaying hadronically. We do not observe any significant peak in the sum of the jet-jet mass distribution of four-jet events. The 95% C.L. upper limits on the production cross-section range from 2.7 to 4.5 pb for $95 \leq (m_X + m_Y) \leq 120$ GeV. We do not observe evidence for associated production of heavy particles with masses around 50–60 GeV.

Acknowledgements

We particularly wish to thank the SL Division for the efficient operation of the LEP accelerator and for their continuing close cooperation with our experimental group. In addition to the support staff at our own institutions we are pleased to acknowledge the
Department of Energy, USA,
National Science Foundation, USA,
Particle Physics and Astronomy Research Council, UK,
Natural Sciences and Engineering Research Council, Canada,
Israel Ministry of Science,
Israel Science Foundation, administered by the Israel Academy of Science and Humanities,
Minerva Gesellschaft,
Japanese Ministry of Education, Science and Culture (the Monbusho) and a grant under the Monbusho International Science Research Program,
German Israeli Bi-national Science Foundation (GIF),
Direction des Sciences de la Matière du Commissariat à l'Energie Atomique, France,
Bundesministerium für Bildung, Wissenschaft, Forschung und Technologie, Germany,
National Research Council of Canada,
Hungarian Foundation for Scientific Research, OTKA T-016660, and OTKA F-015089.

References

[1] ALEPH Collab., D. Buskulic *et al.*, *Four-jet final states production in e^+e^- collisions at centre-of-mass energies of 130 and 136 GeV*, CERN-PPE/96-052, to be published in Z. Phys.

[2] Y. Gol'fand and E. Likhtam, JETP Lett. 13 (1971) 323;
D. Volkov and V. Akulov, Phys. Lett. B46 (1973) 109;
J. Wess and B. Zumino, Nucl. Phys. B70 (1974) 39.

[3] P. Fayet, *Unification of the Fundamental Particle Interactions*, Plenum Press (1980) 587.

[4] OPAL Collab., G. Alexander *et al.*, *Search for Chargino and Neutralino Production Using the OPAL Detector at $\sqrt{s}$ =130 – 136 GeV at LEP*, CERN-PPE/96-020, to be published in Phys. Lett. B.

[5] M. Drees and K. Hikasa, Phys. Lett. B252 (1990) 127;
K. Hikasa and M. Kobayashi, Phys. Rev. D36 (1987) 724.

[6] J. Ellis and S. Rudaz, Phys. Lett. B128 (1983) 248;
G. Altarelli and R. Rückl, Phys. Lett. B144 (1984) 126;
S. Dawson, E. Eichten and C. Quigg, Phys. Rev. D31 (1985) 1581;
J. Ellis, G.L. Fogli and E. Lisi, Nucl. Phys. B393 (1993) 3.

[7] CDF Collab., F. Abe *et al.*, Phys. Rev. D 52 (1995) 2605;
D0 Collab., S. Abachi *et al.*, Phys. Rev. D 52 (1995) 4877.

[8] D0 Collab., S. Abachi *et al.*, Phys. Rev. Lett. 76 (1996) 2228.

[9] D0 Collab., S. Abachi *et al.*, Phys. Rev. Lett. 76 (1996) 2222.

[10] H1 Collab., S. Aid *et al.*, *A search for selectrons and squarks at HERA*, DESY-96-082, May 1996.

[11] ALEPH Collab., D. Buskulic *et al.*, Phys. Lett. B373 (1996) 246;
DELPHI Collab., P. Abreau *et al.*, *Search for the lightest chargino at* $\sqrt{s}$ *= 130 and 136 GeV in DELPHI*, CERN-PPE/96-75, June 1996, submitted to Phys. Lett. B;
L3 Collab., M. Acciarri *et al.*, *Search for Supersymmetric Particles at 130 GeV* $< \sqrt{s} <$ 140 *GeV at LEP*, CERN-PPE/96-29, to be published in Phys. Lett. B.

[12] H. P. Nilles, Phys. Rep. 110 (1984) 1;
H. E. Haber and G. L. Kane, Phys. Rep. 117 (1985) 75.

[13] OPAL Collab., K. Ahmet *et al.*, Nucl. Instr. Meth. A305 (1991) 275;
P. P. Allport *et al.* Nucl. Instr. Meth. A324 (1993) 34;
P. P. Allport *et al.* Nucl. Instr. Meth. A346 (1994) 476.

[14] B.E. Anderson *et al.*, IEEE Transactions on Nuclear Science 41 (1994) 845.

[15] S. Katsanevas, in the LEP200 workshop report, CERN 96/01 (1996).

[16] T. Sjöstrand, Comp. Phys. Comm. 39 (1986) 347;
T. Sjöstrand and M. Bengtsson, Comp. Phys. Comm. 43 (1987) 367;
"PYTHIA 5.6 and JETSET 7.3, Physics and Manual", CERN-TH. 6488/92;
"PYTHIA 5.7 and JETSET 7.4, Physics and Manual", CERN-TH. 7112/93;
T. Sjöstrand, Comp. Phys. Comm. 82 (1994) 74.

[17] A. Bartl, H. Fraas and W. Majerotto, Z. Phys. C30 (1986) 441;
A. Bartl, H. Fraas and W. Majerotto, Z. Phys. C41 (1988) 475;
A. Bartl, H. Fraas, W. Majerotto and B. Mösslascher, Z. Phys. C55 (1992) 257.

[18] A. Ali, Zeit Phys. C1 (1979) 25;
M.K. Gaillard, B.W. Lee and J.L. Rosner, Rev. Mod. Phys. 47 (1975) 227;
V. Barger, T. Gottschalk and R.J.N. Phillips, Phys. Lett. B82 (1979) 445;
M. Suzuki, Nucl. Phys. B258 (1985) 553.

[19] P. Janot, *The HZHA Generator* in *Physics at LEP2*, eds. G. Altarelli, T. Sjöstrand, and F. Zwirner, CERN 96-01 (1996), Vol. 2, p. 309.

[20] R. Bhattacharya, J. Smith, G. Grammer, Phys. Rev. D15 (1977) 3267;
J. Smith, J.A.M. Vermaseren and G. Grammer, Phys. Rev. D15 (1977) 3280.

[21] A. Buijs *et al.*, Comp. Phys. Comm. 79 (1994) 523.

[22] S. Jadach, B. F. L. Ward and Z. Wąs, Comp. Phys. Comm. 79 (1994) 503.

[23] M. Böhm, A. Denner and W. Hollik, Nucl. Phys. B304 (1988) 687;
F.A. Berends, K. Kleiss and W. Hollik, Nucl. Phys. B304 (1988) 712.

[24] D. Karlen, Nucl. Phys. B289 (1987) 23.

[25] The calculation of the cross-section is based on the method described in the preprint by H. Murayama, I. Watanabe and K. Hagiwara, KEK Report 91-11 (1991). The initial state radiation is implemented according to a formula in F. A. Berends, R. Pittau and R. Kleiss, Nucl. Phys. B426 (1994) 344.

[26] F.A. Berends, R. Pittau and R. Kleiss Comput. Phys. Commun. 85 (1995) 437.

[27] J. Allison *et al.*, Nucl. Instr. Meth. A317 (1992) 47.

[28] OPAL Collab., R. Akers *et al.*, Z. Phys. C61 (1994) 19;
OPAL Collab., G. Alexander *et al.*, Z. Phys. C52 (1991) 175.

[29] OPAL Collab., M.Z. Akrawy *et al.*, Phys. Lett. B253 (1991) 511.
In the present analyses an improved parametrisation of the energy measurement is used.

[30] S. Robins, *A Study of Bhabha Scattering at LEP*, Ph.D. Thesis (1992), Queen Mary and Westfield College.

[31] OPAL Collab., R. Akers *et al.*, Phys. Lett. B327 (1994) 411.

[32] OPAL Collab., R. Akers *et al.*, Z. Phys. C60 (1993) 199.

[33] OPAL Collab., P.D. Acton *et al.*, Z. Phys. C60 (1993) 19.

[34] M. Hauschild *et al.*, Nucl. Instr. and Meth. A314 (1992) 74.

[35] OPAL Collab., P. Acton *et al.*, Z. Phys. C58 (1993) 523.

[36] ALEPH Collab., D. Decamp *et al.*, Phys. Lett. B236 (1990) 86;
ALEPH Collab., D. Decamp *et al.*, Phys. Rep. 216 (1992) 253;
L3 Collab., B. Adeva *et al.*, Phys. Lett. B233 (1989) 530;
OPAL Collab., M.Z. Akrawy *et al.*, Phys. Lett. B240 (1990) 1.

[37] C. Peterson, D. Schlatter, I. Schmitt and P.M. Zerwas, Phys. Rev. D27 (1983) 105.

[38] A value of $m_{\mathrm{b}} = 5$ GeV and $\epsilon_{\mathrm{b}} = 0.0047$ from
OPAL Collab., G. Alexander *et al.*, Phys. Lett. B364 (1995) 93, was used.

[39] M.G. Bowler, Z. Phys. C11 (1981) 169.

[40] OPAL Collab., R. Akers *et al.*, Phys. Lett. B337 (1994) 207.

[41] OPAL Collab., Z. Phys. C64 (1994) 1.

[42] OPAL Collab., G. Alexander *et al.*, Z. Phys. C52 (1991) 175.

[43] S. Catani *et al.*, Nucl. Phys. B269 (1991) 432.

[44] OPAL Collab., R. Akers *et al.*, Z. Phys. C65 (1995) 17.

[45] OPAL Collab., G. Alexander *et al.*, *QCD studies with e^+e^- annihilation data at 130 and 136 GeV*, March 1996, CERN-PPE/96-047 (1996), to be published in Z. Phys.

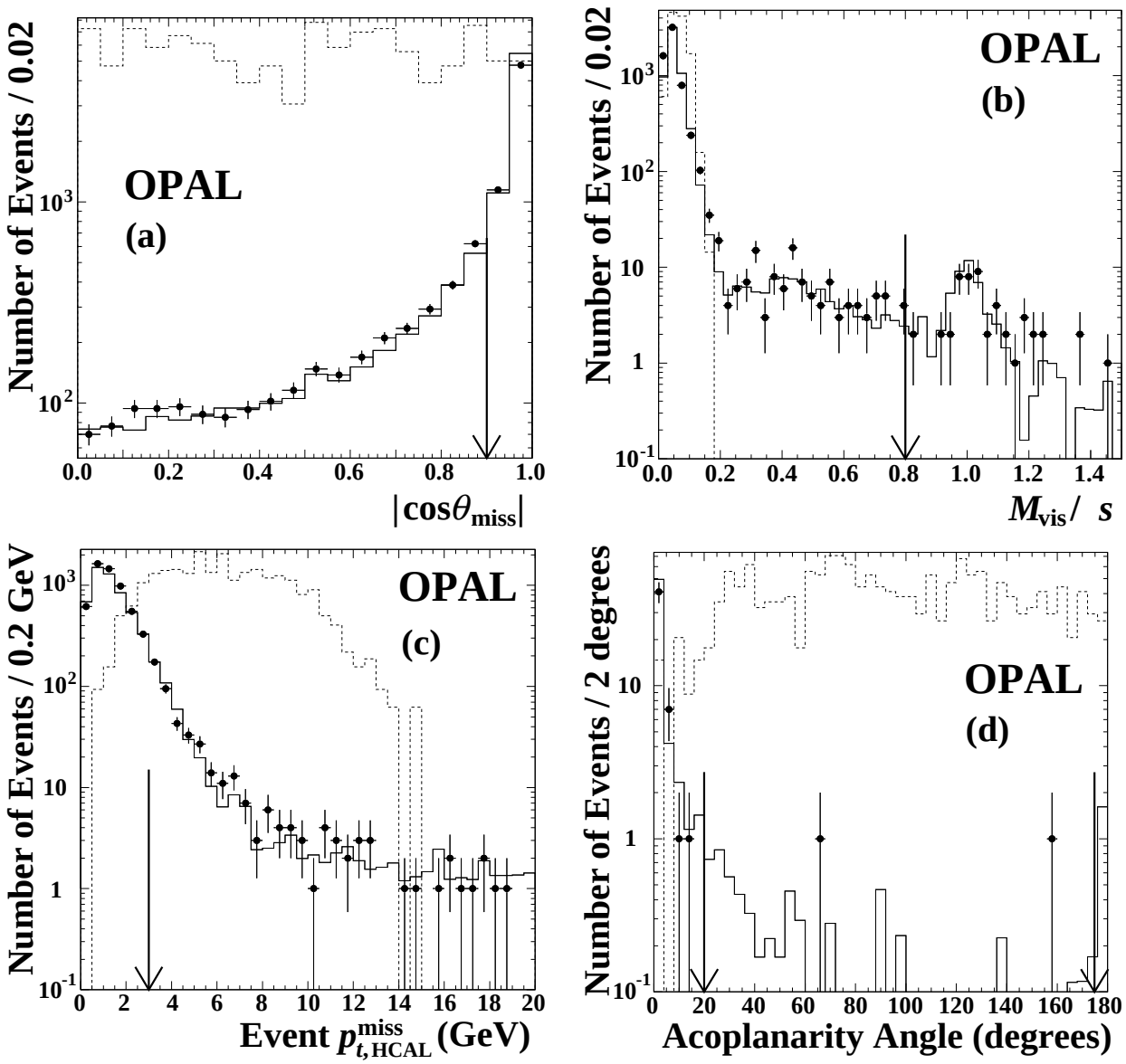

Figure 1: Slepton analysis A: Distributions of (a) the polar angle of the missing momentum direction; (b) the total visible mass of the event; (c) the total p_t of the event including HCAL information; and (d) the acoplanarity angle between the two lepton candidates. Data are shown as points and the sum of all Monte Carlo background processes is shown as a solid line. Distributions are shown after certain cuts have been applied as described in the text. The dashed histogram shows the $\tilde{\mu}^+\tilde{\mu}^-$ Monte Carlo events for $m_{\tilde{\mu}} = 60$ GeV and $m_{\tilde{\chi}_1^0} = 55$ GeV. The simulated signal events are not normalised to the recorded luminosity. The arrows indicate the positions of the cuts.

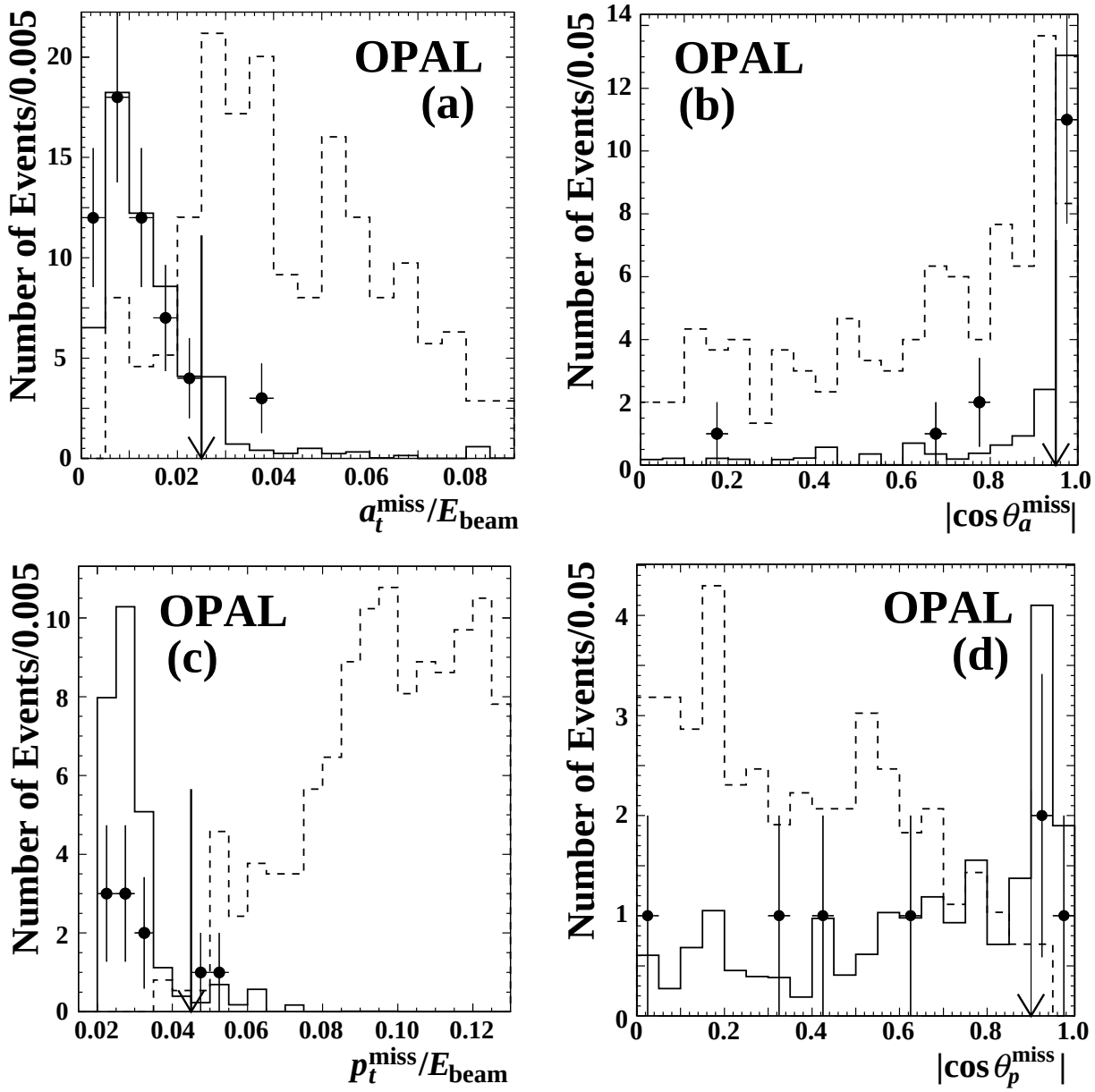

Figure 2: Slepton analysis B: Distributions of cut variables after some of the other selection cuts have been applied: (a) $a_t^{\rm miss}/E_{\rm beam}$ for events with $\phi_{\rm acop} < 1.2$ radians (cut 5b); (b) $|\cos\theta_{\rm a}^{\rm miss}|$ for events with $\phi_{\rm acop} < 1.2$ radians (cut 5c); (c) $p_t^{\rm miss}/E_{\rm beam}$ for events with $\phi_{\rm acop} \geq 1.2$ radians (cut 5d); and (d) $|\cos\theta_{\rm p}^{\rm miss}|$ for events with $\phi_{\rm acop} \geq 1.2$ radians (cut 5e). The data are shown as points with error bars and the Monte Carlo predictions for the Standard Model backgrounds are shown as solid histograms. For comparison, the distributions obtained with a sample of simulated signal events are also shown. The dashed histograms correspond to $\tilde{\mu}^+\tilde{\mu}^-$ events with $m_{\tilde{\ell}} = 60$ GeV and $m_{\tilde{\chi}_1^0} = 55$ GeV, for the case that the decay $\tilde{\ell}^- \rightarrow \tilde{\chi}_1^0 \ell^-$ has a 100% branching ratio. The Standard Model Monte Carlo background events are normalised to the same luminosity as the data. The simulated signal events have arbitrary normalisation. The arrows indicate the positions of the cuts in the event selection.

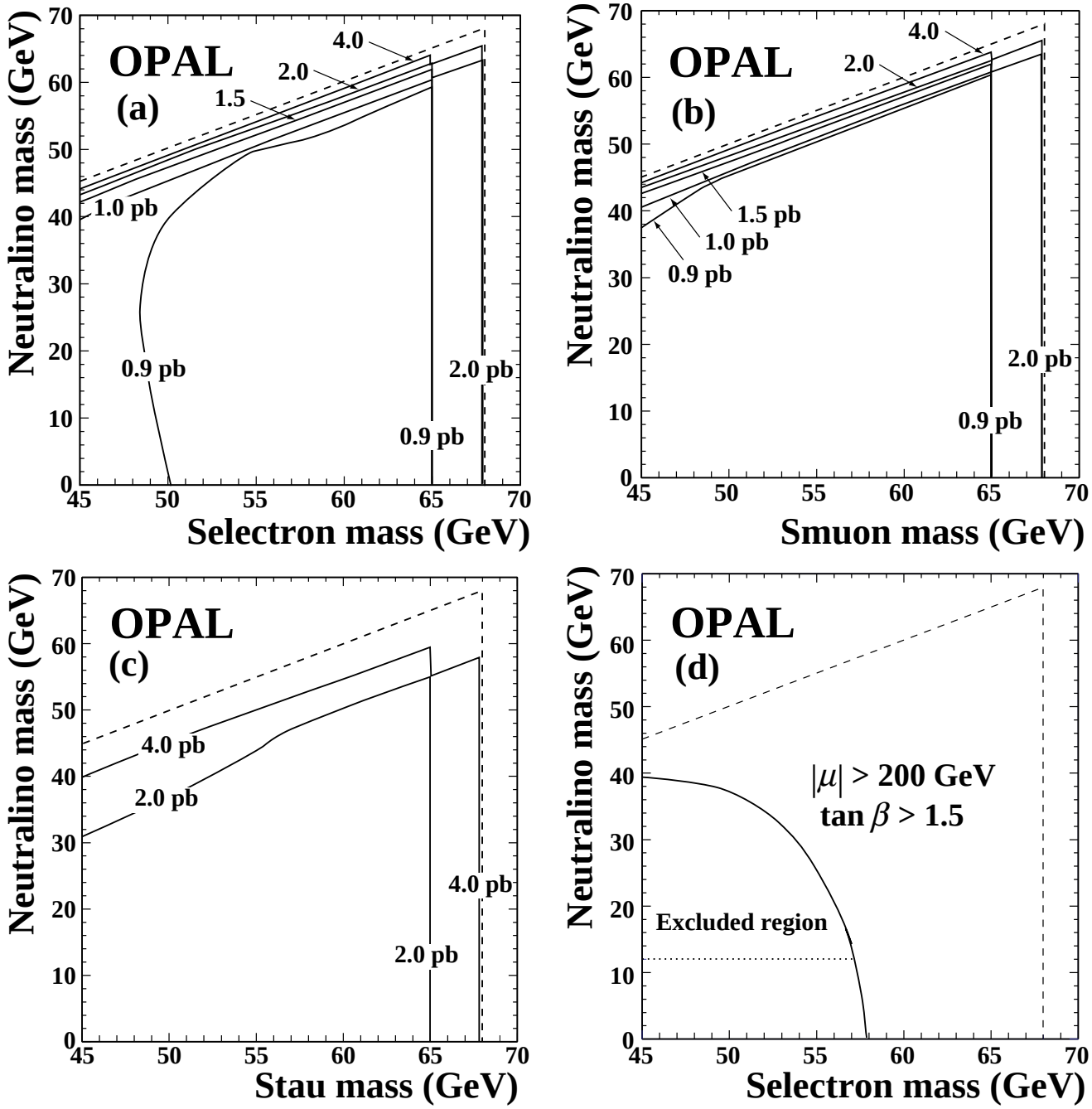

Figure 3: Limits on slepton production. (a)–(c) Model-independent limits for the three slepton species. (d) The MSSM exclusion region for $\tilde{e}_R^+\tilde{e}_R^-$ in the $(m_{\tilde{\chi}_1^0}, m_{\tilde{e}_R})$ plane at 95% C.L. for $\mu = -200$ GeV, $\tan\beta = 1.5$, and using the MSSM predicted branching ratio for $\tilde{\ell}^\pm \to \ell^\pm + \tilde{\chi}_1^0$. The excluded region is valid for all values of $|\mu| > 200$ GeV and $\tan\beta > 1.5$ and corresponds to $M_2 < 80$ GeV. The dotted line shows the current OPAL $\tilde{\chi}_1^0$ lower mass limit [4]. The kinematic limit at $\sqrt{s} = 136$ GeV is shown as the dashed line.

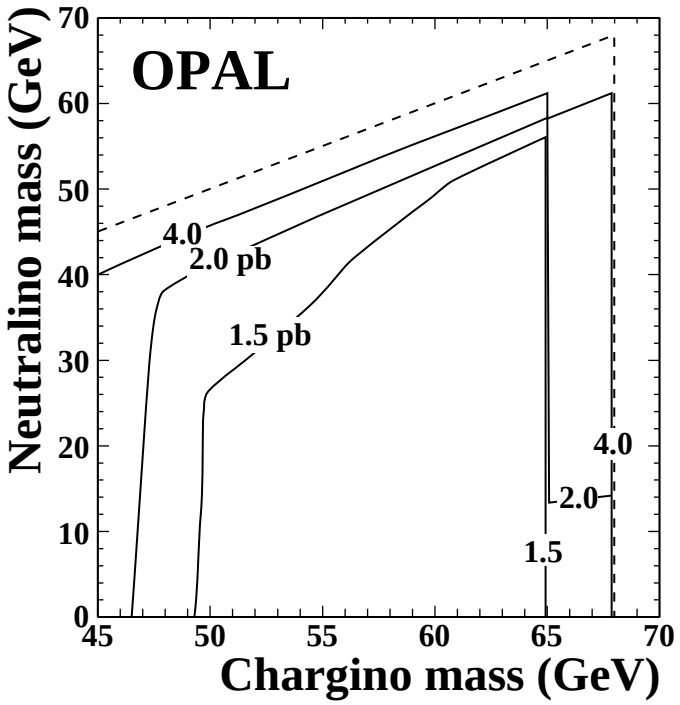

Figure 4: 95% C.L. upper limits on the production cross-section of chargino-pair events with both charginos decaying semileptonically.

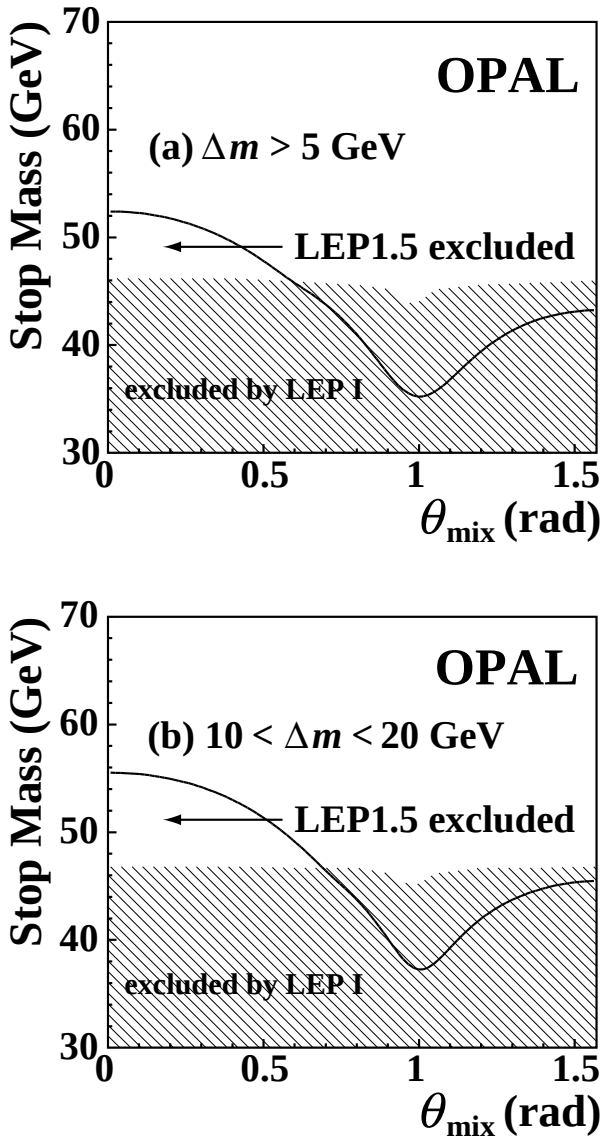

Figure 5: The excluded regions in the ($\theta_{\rm mix}$, $m_{\tilde{t}_1}$) plane at 95% C.L. where the mass differences are assumed to be: (a) $\Delta m (= m_{\tilde{t}_1} - m_{\tilde{\chi}^0_1}) \geq 5$ GeV, (b) $10 \leq \Delta m \leq 20$ GeV. The hatched regions have already been excluded by OPAL [40] using data recorded at the Z^0 peak (LEP 1).

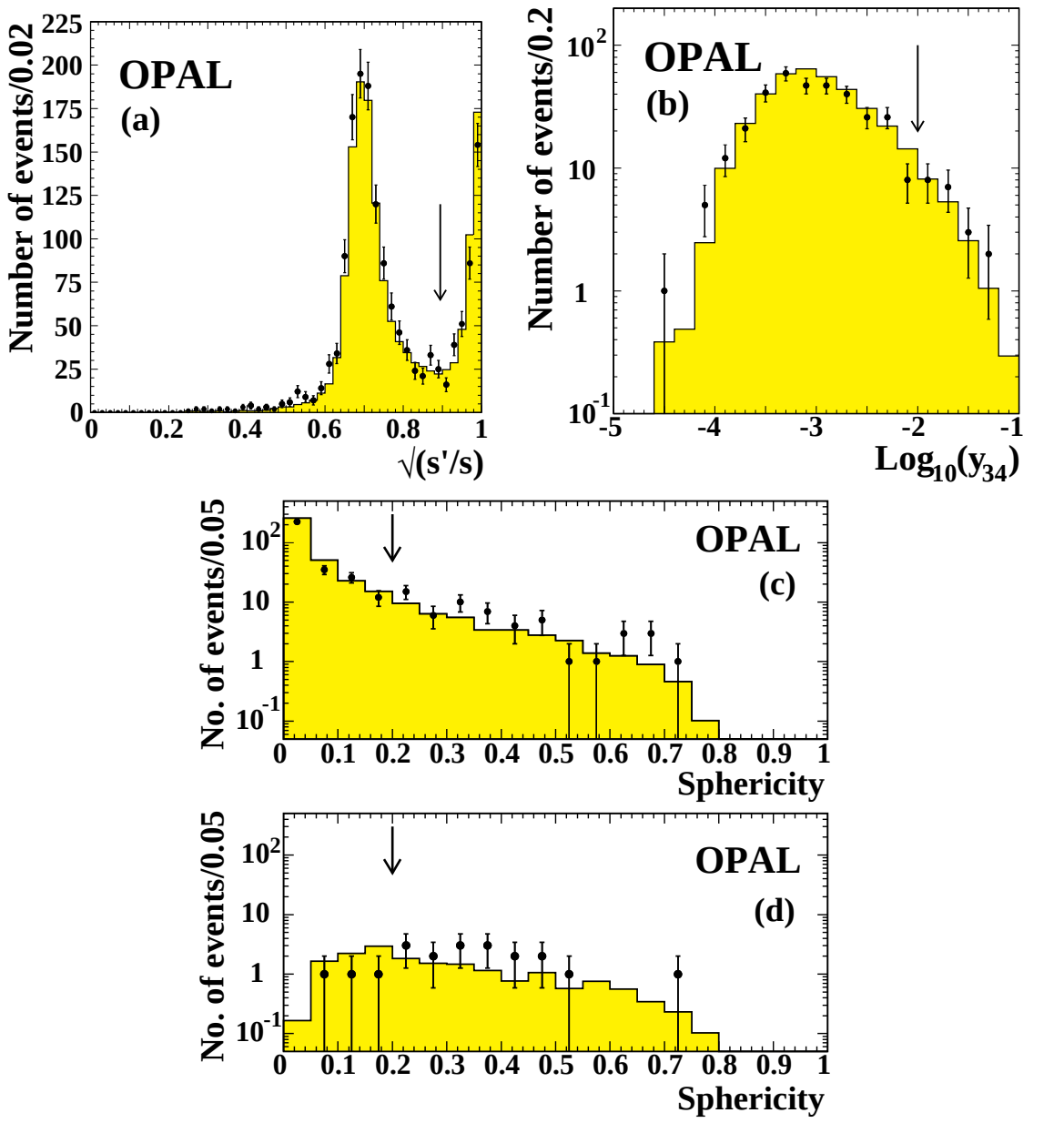

Figure 6: (a) Distribution of $\sqrt{s'/s}$ in multihadronic events in the combined 130 GeV and 136 GeV data set (points with error bars). The histogram shows the expectation from the $q\bar{q}(\gamma)$ Monte Carlo. The arrow shows the position of the cut used to select non-radiative events. (b) Distribution of y_{34}, the value of y_{cut} in the Durham jet-finding scheme at which an event changes from three to four jets, for multihadronic events with $s'/s \geq 0.8$. The arrow shows the cut used to select four-jet events. (c) Sphericity distribution for multihadronic events with $s'/s \geq 0.8$. The histogram shows the distribution for $q\bar{q}$ Monte Carlo events. (d) The same as (c), but additionally applying the cut $y_{34} \geq 0.01$. The arrows show the positions of the cuts.

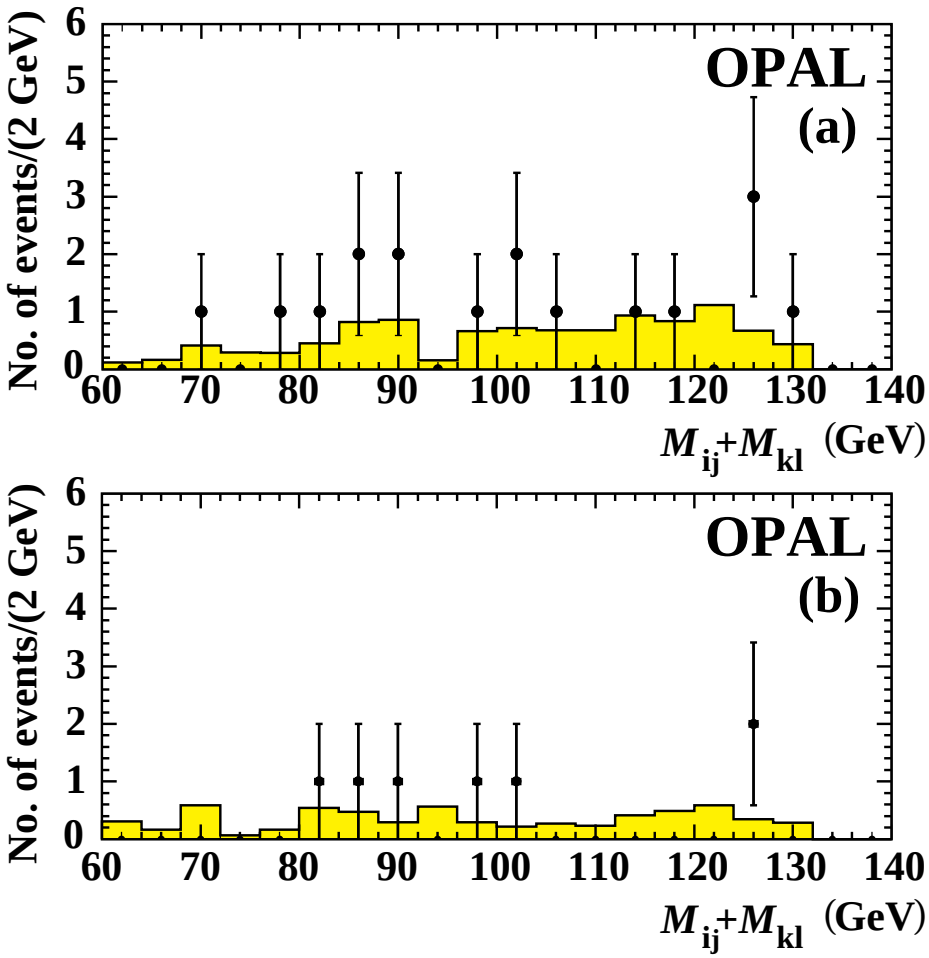

Figure 7: (a) Sum of the two reconstructed jet-jet masses for events with $s'/s \geq 0.8$, $y_{34} \geq 0.01$ and sphericity $S \geq 0.2$ (first set of selection criteria). The combination with the minimum difference between the two masses is plotted. The histogram shows the expectation from the $q\bar{q}(\gamma)$ Monte Carlo (no b-tagging is required). (b) Sum of the two reconstructed jet-jet masses for events passing the second set of selection criteria. The combination with the minimum difference between the two masses is plotted. The histogram shows the expectation from the $q\bar{q}$ Monte Carlo (no b-tagging is required).

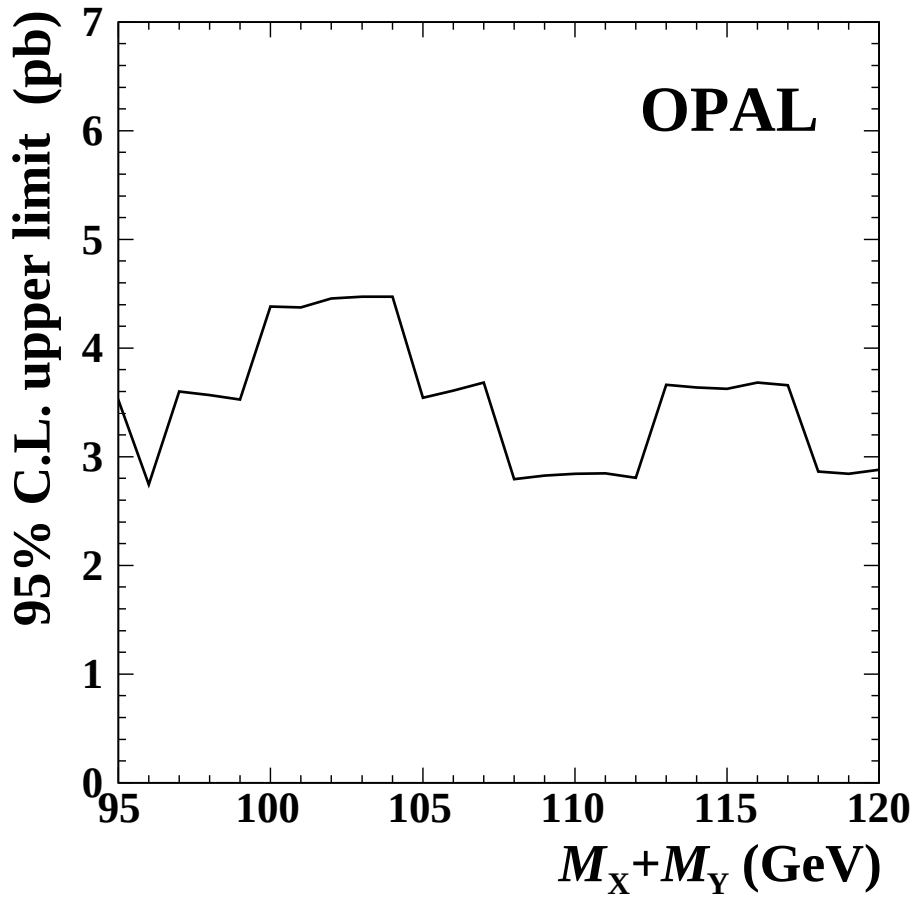

Figure 8: 95% C.L. cross-section upper limits for the process $e^+e^- \rightarrow XY$, with both X and Y decaying into quarks. These limits are derived from the first analysis described in subsection 7.2 (no b-tagging is required).